

# CNO in evolved intermediate mass stars <sup>★</sup>

R. Smiljanic<sup>1</sup>, B. Barbuy<sup>1</sup>, J. R. De Medeiros<sup>2</sup>, and A. Maeder<sup>3</sup>

<sup>1</sup> Universidade de São Paulo, IAG, Rua do Matão 1226, Cidade Universitária, 05508-900, São Paulo, SP, Brazil  
e-mail: rodolfo@astro.iag.usp.br, barbuy@astro.iag.usp.br

<sup>2</sup> Universidade Federal do Rio Grande do Norte, Departamento de Física, Campus Universitário, 59072-970, Natal, RN, Brazil  
e-mail: renan@dfte.ufrn.br

<sup>3</sup> Geneva Observatory, 1290 Sauverny, Switzerland  
e-mail: Andre.Maeder@obs.unige.ch

Received / Accepted

**Abstract.** In order to investigate the possible influence of rotation on the efficiency of the first dredge-up we determined atmospheric parameters, masses, and abundances of carbon, nitrogen, and oxygen in a sample of evolved intermediate mass stars. We used high resolution spectra and conducted a model atmosphere analysis. The abundances were calculated through spectral synthesis and compared to the predictions of rotating and non-rotating evolutionary models. Almost all those objects in our sample where carbon and nitrogen abundances could be determined show signs of internal mixing. The stars, however, seem to be mixed to different extents. Among the mixed stars we identify five in our sample with abundances in agreement with the non-rotating models, four stars that seem to be mixed beyond that, and one star that seems to be slightly less mixed than predicted for the first dredge-up. There are also five stars that seem to be slightly more mixed than expected, but their abundances are in marginal agreement with both rotating and non-rotating models. Such differences in the extent of the mixing are not predicted by the standard models and imply the action of other mixing mechanisms than solely the convective dredge-up. We also identified for the first time an important correlation between the [N/C] ratio and the stellar mass.

**Key words.** Stars: fundamental parameters – Stars: abundances – Stars: supergiants – Stars: rotation

## 1. Introduction

The evolution of a star is usually treated as a function only of initial mass and chemical composition. Issues such as rotation and magnetic fields are considered as playing a minor role. However, in the past few years discrepancies have been found between model predictions and the observations of abundances in intermediate mass stars ( $5\text{-}20M_{\odot}$ ), which could be due to the earlier neglect of rotation.

Intermediate mass stars burn hydrogen during the main sequence (MS) via the CNO cycle. One of the main outcomes of the CNO cycle is the conversion of almost all central  $C^{12}$  into  $N^{14}$ . When the central hydrogen is exhausted, the star expands its outer layers and cools off, evolving rapidly to the red giant branch (RGB). Before it starts to burn He, the star experiences the so-called first dredge-up, the development of a deep convective layer that brings nuclear processed material to the surface. The photospheric abundances of carbon and nitrogen are then altered (C is reduced and N is increased).

During the RGB, depending on its mass, the star can experience a blue-loop; in the models by Schaller et al. (1992) the evolutionary tracks for stars between 5 and 12  $M_{\odot}$  have blue

loops. The star evolves from the RGB to the blue-giant region, due to a temporary increase in the effective temperature, and then back to the RGB. The occurrence and extent of the loop are dependent on the mass and on other uncertain factors, such as the treatment of convection. More details on the blue loops can be found in Xu & Li (2004) and references therein. Since the first crossing of the HR diagram, from the MS to the RGB, happens on a short time scale of a few million years, most of the stars observed in the blue giant region must be evolving through a blue loop.

In spite of this relatively simple description, the observations reveal a more complex scenario. Although an important mixing episode is not supposed to happen before the first dredge-up there is evidence of He (Lyubimkov 1998) and N (Gies & Lambert 1992 and Lennon et al. 1996) overabundances in O and B stars. In addition, boron seems to be highly depleted in main sequence B stars (Venn et al. 2002). These are probable indications of mixing during the MS. In particular, Fliegner et al. (1996) show that it is possible to qualitatively reproduce the boron behavior by including rotation effects in theoretical evolutionary calculations.

On leaving the MS, as well as during the blue loop, the stars will eventually shine as A type stars. Venn (1995a, b) analyzed a sample of Galactic A-type supergiants and found stars with

Send offprint requests to: B. Barbuy

<sup>★</sup> Observations collected at ESO, La Silla, Chile

unchanged composition, as well as stars with slightly modified composition. These stars are probably crossing the HR diagram for the first time and the latter group might be reflecting a mixing episode that occurred during the MS. Venn (1999) analyzed A-type supergiants from the SMC where some stars showed signs of the first dredge-up and others were non-mixed. The nitrogen abundance in the post first dredge-up stars shows a spread that is not predicted by the models. This spread might probably be due to different rotations inducing different mixing efficiencies.

There are only a few abundance determinations in yellow (F-G) and red (K-M) supergiants. Sodium overabundances were detected (Boyarchuk & Lyubimkov 1983) and they appear to be correlated with mass (Sasselov 1986). The Na overabundances are probably related to the operation of the Ne-Na cycle during hydrogen burning. El Eid & Champagne (1995) have investigated the Ne-Na cycle theoretically in A-F supergiants and their results agree well with observations.

Luck & Lambert (1985) determined C, N, and O abundances in a sample of 2 variables and 4 non-variables F supergiants. They found a higher N/C ratio than expected (more N and less C), which is an indication of a more efficient mixing in these stars. Barbuy et al. (1996) have determined C, N, and O abundances in a sample of 9 low-rotator F supergiants. They found stars with non-modified abundances and stars with abundances that are only slightly changed.

There are also some determinations of C and N abundances in Cepheid stars (Andrievsky et al. 1996, 2002, 2004, Luck et al. 2003, Kovtyukh et al. 1996, Usenko et al. 2001a, b). In general there are stars without changes in their abundances, which are probably crossing the instability strip for the first time, stars with  $[N/C]$  near the expected value for the first dredge-up, and stars with abundances changed beyond what is expected. The last group of stars has probably passed through more efficient mixing processes. It is worth noting that Kovtyukh et al. (1996) have found two stars overabundant in Na but with normal abundances of C and N.

Consequently, the scenario suggested by the observations is much more complex than predicted by the standard models. Two characteristics in particular must be stressed. The first is the indication of mixing processes during the MS. The second is the indication of a more efficient mixing than the expected solely due to the first dredge-up. Neither are predicted by the standard non-rotating models. The inclusion of rotation in the models seems to be able to reproduce these behaviors at least qualitatively.

Much effort has been made in the last years towards a better physical treatment of rotation and its effects, as reviewed by Maeder & Meynet (2000) and references therein. Effects induced by rotation, such as meridional circulation (Maeder & Zahn 1998) and especially shear turbulence (Maeder 1997; Mathis et al. 2004; Mathis & Zahn 2004) act in transporting and mixing the chemical elements. Thus the required additional mixing mechanism seems to appear naturally when rotation effects are taken into account. Even a mixing event during the MS should happen if the rotation is sufficiently high. Although this seems promising, much work still needs to be done. More ob-

servational results are very needed in order to better constrain the models.

In this work we derive C, N, and O abundances in a sample of cool giants and supergiants. The observations are described in Sect. 2, the stellar parameters are described in Sect. 3, and the abundances of CNO are described in Sect. 4. The results are discussed in Sect. 5 and conclusions drawn in Sect. 6.

## 2. Observations

High resolution CCD spectra were obtained for a sample of 19 cool luminous stars using the FEROS spectrograph at the ESO 1.52m telescope at La Silla (Chile). FEROS is a fiber-fed echelle spectrograph that provides a full wavelength coverage of  $\lambda\lambda$  3500-9200 Å over 39 orders at a resolving power of  $R=48,000$  (Kaufer et al. 2000). The detector used was an EEV CCD chip with 2048x4096 pixels and with a pixel size of  $15\mu\text{m}$ . The program stars were observed during four observational runs in 2000 and 2001, as given in Table 1. All spectra were reduced using the FEROS pipeline software.

An estimation of the average signal to noise ratio for each spectrum is given in Table 1. This table also lists the spectral type, visual magnitude, galactic coordinates, parallax, heliocentric radial velocity, and rotational velocity of the program stars. The rotational velocities were mainly taken from De Medeiros et al. (2002) with the exception of HD 80404 from Royer et al. (2002) and HD 38713 and HD 45348 from De Medeiros (2005, private communication). The radial velocities were determined using IRAF. The other stellar data in Table 1 were taken from Simbad<sup>1</sup>.

The equivalent widths of FeI and FeII lines were determined by fitting Gaussian profiles to the lines with IRAF, and in the analysis, lines with equivalent widths larger than  $150\text{m}\text{\AA}$  were not used. For the three hottest stars, HD 36673, HD 45348, and HD 80404, no lines larger than  $100\text{m}\text{\AA}$  were used.

## 3. Stellar parameters

### 3.1. Physical data

Oscillator strengths for FeI lines were preferred from the NIST database (Martin et al. 2002) complemented by the list used by Barbuy et al. (1996). For the FeII lines the oscillator strengths were mainly taken from Meléndez & Barbuy (2005) complemented by Barbuy et al. (1996) and Kovtyukh & Andrievsky (1999). The equivalent widths and oscillator strengths are listed in the Appendix (Tables 12, 13, 14, and 15).

In this analysis we used grids of model atmospheres generated by the ATLAS9 code (Kurucz 1994) for stars hotter than 4750K, whereas grids of model atmospheres by the NMARCS code (Plez et al. 1992) were adopted for the cooler stars. The ATLAS9 models assume local thermodynamic equilibrium (LTE), plane-parallel geometry, and hydrostatic equilibrium. The NMARCS models are spherically symmetric and assume LTE and hydrostatic equilibrium. The NMARCS models are a

<sup>1</sup> This research made use of the Simbad database operated at the CDS, Strasbourg, France.

**Table 1.** Sample stars: HD number, spectral type, visual magnitude, galactic coordinates, parallax, rotational velocity, heliocentric radial velocity of the stars, signal to noise ratio and, date of observation.

HD	ST	$V$	$b$	$l$	$\pi$	$v \sin i$ km s <sup>-1</sup>	$V_r^{hel.}$ km s <sup>-1</sup>	$S/N$	Date of obs.
1219	K1IV	8.91	-64.6°	315.7°	5.30	–	-19.6	250	10.19.2000
36673	F0Ib	2.60	-25.1°	220.9°	2.54	10.0	2.4	450	02.17.2000
38713	G8III	6.17	-21.4°	220.8°	4.91	2.3	6.3	300	01.15.2001
44362	G2Ib	7.04	-25.6°	258.5°	1.24	8.8	14.9	320	01.15.2000
45348	F0II	-0.72	-25.3°	261.2°	10.43	8.0	20.6	420	01.15.2000
49068	K0-III	7.43	-10.6°	231.1°	2.18	<1.0	23.8	400	01.15.2000
49396	G6Iab	6.55	-22.0°	261.6°	1.49	8.6	29.4	290	01.15.2000
51043	G5Ib-II	6.56	-21.5°	263.9°	2.36	3.5	14.3	210	01.15.2000
66190	K1Ib-II	6.61	-8.1°	260.4°	0.60	4.0	27.4	360	01.15.2000
71181	G6Ib-II	7.62	-4.4°	262.4°	-1.80	2.1	13.5	550	02.14.2000
76860	K3Ib	7.14	-2.7°	269.4°	0.43	2.0	4.5	460	01.16.2001
80404	A8Ib	2.25	-7.0°	278.5°	4.71	10.0	10.9	330	01.16.2001
90289	K4III	6.34	-0.5°	284.4°	4.11	<1.0	-16.1	250	01.14.2001
102839	G5Ib	4.98	-8.0°	297.7°	2.24	7.6	14.2	240	02.14.2000
114792	F5-F6Ib	6.85	+0.1°	305.4°	0.36	7.5	-17.5	410	02.14.2000
159633	G2Ib	6.27	-3.4°	351.3°	1.15	9.1	11.6	310	10.04.2001
192876	G3Ib	4.25	-24.7°	31.1°	4.75	7.3	-27.4	350	10.20.2000
204867	G0Ib	2.91	-37.9°	48.0°	5.33	9.5	6.1	360	10.20.2000
225212	K3Iab	4.95	-70.0°	87.1°	2.03	5.8	-42.0	320	10.19.2000

more suitable choice for the cooler stars for its better description of the opacity sources. Whenever necessary, codes for interpolating among the grids were adopted.

### 3.2. Effective temperature

For each star we derived the effective temperature using four different approaches: the excitation equilibrium of FeI lines, the excitation equilibrium of FeII lines, photometric calibrations, and fitting the H $\alpha$  line wings. Using each temperature estimate, we calculated the complete set of atmospheric parameters, namely surface gravity ( $\log g$ ), microturbulence velocity ( $\xi$ ) and, metallicity ([Fe/H]). After a comparison we chose the more reliable set of parameters as described below.

#### 3.2.1. $T_{\text{eff}}$ from FeI

In the derivation of the  $T_{\text{eff}}$  from the FeI lines, all the parameters were calculated simultaneously. In this method the  $T_{\text{eff}}$  was found by requiring a null correlation of the iron abundance as given by the FeI lines with the excitation potential (the excitation equilibrium). The surface gravity was found by requiring both FeI and FeII lines to have the same mean abundance (the ionization equilibrium). The microturbulence velocity was found by requiring the iron abundance (from FeI lines) to have a null correlation with the equivalent widths. By fulfilling these conditions we also determined the iron abundance, [Fe/H].

Usually one adopts FeI for this kind of analysis because it is a chemical species with a high number of lines available in the spectrum. However, there is evidence that it must be adopted with care in some cases. Lyubimkov & Boyarchuk (1983) argue that in F supergiants FeI might be overionized due to non-LTE effects; FeII, on the other hand, should not be affected.

When computing the parameters with the FeI lines, we noticed a tendency for the hotter stars to have higher metallicities (around [Fe/H] = +0.3 dex). In particular, the three stars with earlier spectral type, HD 36673 (F0), HD 45348 (F0), and HD 80404 (A8) showed metallicities larger than [Fe/H] = +0.50 dex. These results do not seem to be reasonable and are probably spurious due to NLTE effects. Since FeII is probably not affected by NLTE (Lyubimkov & Boyarchuk 1983), its use to constrain the parameters should produce more reliable results (Kovtyukh & Andrievsky 1999).

#### 3.2.2. $T_{\text{eff}}$ from FeII

The parameters were recalculated through the same steps described using FeI. The main obstacle in using FeII lines is their reduced number. The number of lines used in this work varies from 6 to 18 per star. A small set of lines containing one or two unreliable lines, affected by blends or by uncertain  $gfs$ , can generate unreliable correlations, thus leading to uncertain parameters. That was probably the case for the stars HD 66190, HD 76860, and HD 102839, for which we found metallicities larger than [Fe/H] = +0.60 dex. According to the FeI parameters, these are cool stars where there are more blends.

However there are two points worth noting. First, the parameters for the three hotter stars, as derived from the FeII lines, show a good agreement with the parameters in the literature. Second, in general the metallicities obtained in this way are smaller than the ones obtained with the FeI lines. This is mainly due to a larger  $\xi$  and a slightly lower  $T_{\text{eff}}$  obtained from the FeII lines.

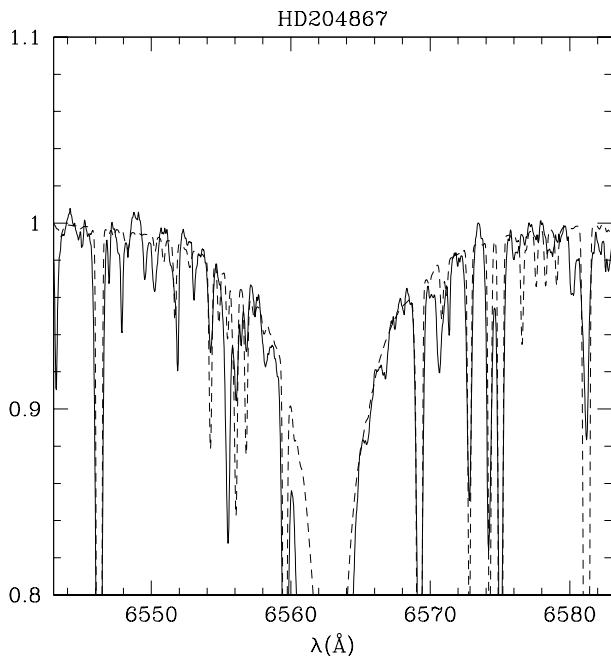


**Fig. 1.** Fit to  $H\alpha$  wings in HD 204867, the dashed line is the synthetic spectrum, and the continuous line is the observed one.

### 3.2.3. $T_{\text{eff}}$ from $H\alpha$

The wings of hydrogen lines are good temperature indicators considering they are independent of  $\log g$  and  $\xi$  for a large range of temperatures. We estimated the  $T_{\text{eff}}$  by fitting the  $H\alpha$  wings with synthetic spectra.

In this method synthetic  $H\alpha$  profiles are calculated for a variety of temperatures until a best fit to the observed profile is found. The synthetic spectra were calculated by programs described in Barbuy et al. (2003), and the hydrogen line profile was calculated with an improved version of the code presented by Praderie (1967). The programs calculate the  $H\alpha$  profile and the lines that contaminate its wings. An example of the fit is given in Fig. 1.

For cooler stars than 4900K, the  $H\alpha$  line has no pronounced wings to be fitted, hence the temperature could be determined in this way only for the hotter ones. At gravities below 2.5 dex and higher temperatures than 7000K, the  $H\alpha$  line becomes sensitive to both  $T_{\text{eff}}$  and  $\log g$ . Three of our stars, HD 45348, HD 36673, and HD 80404, are in these conditions, so an independent estimate for the  $\log g$  is then required. For these stars we chose the best fit with the  $\log g$  as close as possible to the one derived when adopting the  $T_{\text{eff}}$  and  $\xi$  from the FeII lines as discussed above.

### 3.2.4. $T_{\text{eff}}$ from photometry

We also calculated a photometric estimate of the effective temperature using the  $(V - K)$  calibrations of McWilliam (1991), Van Belle et al. (1999), and Houdashelt et al. (2000). A mean value was calculated by adopting no weight difference. The calibration of McWilliam (1991) is valid for F supergiants but the calibrations of Van Belle et al. (1999) and Houdashelt et al.

(2000) are appropriate for giant stars. In spite of that we noticed a very good agreement between the temperatures derived from both calibrations as can be seen in Table 2.

Visual magnitudes were obtained from Simbad and  $K_s$  magnitudes from 2MASS (Cutri et al. 2003). The  $K_s$  magnitudes were transformed into Johnson  $K$  magnitudes by means of the relations from Alonso et al. (1998). Interstellar visual extinction,  $A_V$ , was calculated using the relations from Chen et al. (1998) for stars with  $|b| < 10^\circ$  and  $d < 1kpc$ , and the relations from Hakkila et al. (1997) for the other ones. In both cases the visual extinction is calculated given the galactic coordinates and distance. The distances were calculated using the parallaxes from the Hipparcos catalogue (ESA 1997) or from the Tycho catalogue (ESA 1997) whenever measurements from Hipparcos were not available. Visual extinctions were transformed into color excesses adopting  $A_V/E(B - V) = 3.10$  as the ratio of total to selective absorption. In order to deredden the color  $(V - K)$  we used the expression from Rieke & Lebofsky (1985),  $E(V - K) = 2.744E(B - V)$ . The extinction,  $A_V$  and the dereddened color,  $(V - K)_0$  are listed in Table 2.

For one star in particular, HD 114792, the color excess was calculated using a different approach. The Hipparcos parallax indicates a distance of  $d = 2.78kpc$  and, since it is located in the Galactic Plane, the formula from Hakkila et al. predicts a rather high extinction,  $A_V = 4.02mag$ . By using this extinction one obtains a high effective temperature,  $T = 11000K$ . However, by visual inspection, its spectrum is not of a hot star. Thus we concluded that the distance estimate is not adequate and a distance-independent color excess should be a better approach. We then adopted the  $E(B - V)$  calibration of Strömgren photometry from Arellano-Ferro & Parrao (1990).

### 3.3. Surface gravity

Each temperature estimate was used to calculate a set of atmospheric parameters. In all cases the surface gravity was calculated by requiring the ionization equilibrium of FeI and FeII. The only exceptions were made when using the  $T_{\text{eff}}$  from  $H\alpha$  for the stars HD 36673, HD 45348, and HD 80404. In these cases we tried to keep the gravity as close as possible to the value derived when  $T_{\text{eff}}$  and  $\xi$  were determined from the FeII lines. However, the value usually needed to be adjusted during the fit itself. With a fixed  $\log g$  the wings of the line do not grow indefinitely with increasing  $T_{\text{eff}}$ . There is a maximum, given that further increasing of the  $T_{\text{eff}}$  will diminish the intensity of the wings. Thus, it was not always possible to keep the exact value of  $\log g$ , so some adjustments were necessary.

### 3.4. Microturbulence

We determined the microturbulence from both FeI and FeII lines by requiring the abundances to have a null correlation with the equivalent width. Thus, up to six different sets of parameters were calculated for each star: i)  $T_{\text{eff}}$  and  $\xi$  from FeI lines, ii)  $T_{\text{eff}}$  and  $\xi$  from FeII lines, iii)  $T_{\text{eff}}$  from photometric calibrations and  $\xi$  from FeI lines, iv)  $T_{\text{eff}}$  from photometric calibrations and  $\xi$  from FeII lines, v)  $T_{\text{eff}}$  from  $H\alpha$  and  $\xi$  from FeI

**Table 2.** Interstellar extinction, dereddened color  $(V - K)_0$ , photometric estimates of the effective temperature as calculated from the indicated calibrations and mean values.

HD	$A_V$	$(V - K)_0$	$T_{\text{eff}}(V - K)$ McWilliam(1991)	$T_{\text{eff}}(V - K)$ vanBelle(1999)	$T_{\text{eff}}(V - K)$ Houdashelt(2000)	Final $T_{\text{eff}}$
1219	0.03	2.43	–	4696	4685	4691
36673	0.08	0.73	6971	–	6975	6973
38713	0.07	1.86	–	5162	5295	5229
44362	0.09	1.77	5069	5251	5411	5244
45348	0.08	0.47	7446	–	7448	7447
49068	0.11	2.68	–	4525	4468	4497
49396	0.17	1.93	–	5101	5214	5157
51043	0.17	2.21	–	4864	4903	4884
66190	0.50	2.23	–	4851	4886	4868
71181	0.24	2.44	–	4691	4678	4685
76860	1.49	2.63	–	4563	4515	4539
80404	0.07	0.62	7173	–	7172	7173
90289	0.10	3.38	–	4136	4029	4082
102839	0.25	2.74	–	4489	4423	4456
114792	1.02	1.44	5662	–	–	5662
159633	1.17	1.50	5562	–	5766	5664
192876	0.25	2.06	–	4984	5061	5023
204867	0.11	1.56	5446	5456	5679	5527
225212	0.08	3.45	–	4105	3999	4052

lines, and vi)  $T_{\text{eff}}$  from  $H\alpha$  and  $\xi$  from FeII lines. When comparing the parameters with the same  $T_{\text{eff}}$  but different  $\xi$ , we noticed that the  $\xi$  from the FeII lines is usually larger, hence the metallicity is usually smaller.

### 3.5. Adopted parameters

Final atmospheric parameters were chosen among the six different estimates described above. Among all the methods used to estimate the  $T_{\text{eff}}$ , the  $H\alpha$  fitting is the most reliable. It has problems with neither NLTE nor reddening corrections, despite some uncertainty coming from the model atmosphere (Castilho et al. 2000). Thus we adopted the  $T_{\text{eff}}$  from  $H\alpha$  for all those stars where it could be determined. Moreover, since the FeI lines are not reliable for determining  $\xi$  in the hot stars, we adopted the  $\xi$  as given by the FeII lines for all those stars for which  $T_{\text{eff}}$  was derived from  $H\alpha$ .

For the cool stars, where  $H\alpha$  fitting was not possible, we adopted the parameters as given by the FeI lines. In these stars NLTE is not expected to be significant, and the FeII proved not to inspire much confidence, probably because of an increased number of blends.

There was only one exception. Even though HD 1219 is a cool star, we adopted the parameters as given by the FeII lines. This choice was made because the parameters derived from the FeI lines proved unreliable. The metallicity as derived from FeI lines was  $[\text{Fe}/\text{H}] > +0.50$  dex. Table 3 lists the adopted parameters and the method of calculation.

### 3.6. Uncertainties of the parameters

In order to estimate the uncertainties of the parameters, we divided the stars in two groups, the first for stars where the  $T_{\text{eff}}$

**Table 4.** Uncertainties in the adopted atmospheric parameters.

HD	$T_{\text{eff}}$	$\log g$	$\xi$
49396	$\pm 200\text{K}$	$\pm 0.25\text{dex}$	$\pm 0.35\text{km s}^{-1}$
76860	$\pm 200\text{K}$	$\pm 0.40\text{dex}$	$\pm 0.20\text{km s}^{-1}$

is from  $H\alpha$  fitting and  $\xi$  from the FeII lines and the second for stars whose parameters were all calculated from the FeI lines. We then chose a representative star, with the parameters close to the mean ones of its group, and calculated the uncertainties using them. The uncertainties thus calculated were then extended to the entire group. The chosen stars are HD 49396 and HD 76860.

When determining the  $T_{\text{eff}}$  from the FeI lines, we searched for a linear fit where the angular coefficient is null. Obviously this coefficient has a statistical uncertainty. In order to find the  $1\sigma$  uncertainty on the  $T_{\text{eff}}$  determination we changed the temperature until the angular coefficient of the linear fit matched its own uncertainty. A similar procedure was followed to find the uncertainty on the  $\xi$  determination. The uncertainties thus calculated are listed in Table 4.

In order to find the uncertainty of the  $T_{\text{eff}}$  in the star HD 49396, we had to follow a different procedure. For this star the  $T_{\text{eff}}$  was determined from the  $H\alpha$  fitting. We then changed the temperature until the calculated fit marginally agreed with the observed profile. In this sense, any fit with temperature between these limits could be considered somewhat reasonable.

In order to find the  $1\sigma$  uncertainty of the surface gravity, we proceeded as follows. The mean abundance as given from the FeI lines and from the FeII lines have, in general, different standard deviations. The uncertainties here are considered to be the standard deviations. We then changed the gravity until the

**Table 3.** Adopted atmospheric parameters.

HD	$T_{\text{eff}}$ (K)	log g	$\xi$ km s <sup>-1</sup>	[FeI/H] $\pm\sigma$ (#)	[FeII/H] $\pm\sigma$ (#)	method
1219	4400	1.90	1.25	+0.19 $\pm$ 0.08 (46)	+0.18 $\pm$ 0.17 (15)	$T_{\text{eff}}$ and $\xi$ from FeII
36673	7450	1.90	4.70	0.00 $\pm$ 0.16 (32)	0.00 $\pm$ 0.07 (12)	H $\alpha$ and $\xi$ from FeII
38713	5100	2.45	1.63	+0.05 $\pm$ 0.08 (62)	+0.06 $\pm$ 0.07 (18)	H $\alpha$ and $\xi$ from FeII
44362	5600	1.55	3.09	+0.10 $\pm$ 0.09 (32)	+0.09 $\pm$ 0.26 (07)	H $\alpha$ and $\xi$ from FeII
45348	7450	2.10	3.30	-0.04 $\pm$ 0.21 (35)	-0.13 $\pm$ 0.05 (13)	H $\alpha$ and $\xi$ from FeII
49068	4625	2.20	1.78	+0.19 $\pm$ 0.08 (47)	+0.19 $\pm$ 0.17 (17)	$T_{\text{eff}}$ and $\xi$ from FeI
49396	5350	2.15	5.03	+0.14 $\pm$ 0.11 (26)	+0.13 $\pm$ 0.03 (06)	H $\alpha$ and $\xi$ from FeII
51043	4900	1.85	2.74	+0.02 $\pm$ 0.11 (34)	+0.02 $\pm$ 0.08 (12)	H $\alpha$ and $\xi$ from FeII
66190	4785	1.85	2.67	+0.26 $\pm$ 0.10 (34)	+0.25 $\pm$ 0.07 (14)	$T_{\text{eff}}$ and $\xi$ from FeI
71181	5100	2.30	2.59	+0.14 $\pm$ 0.14 (55)	+0.13 $\pm$ 0.06 (12)	H $\alpha$ and $\xi$ from FeII
76860	4375	1.75	2.67	+0.17 $\pm$ 0.13 (38)	+0.17 $\pm$ 0.18 (13)	$T_{\text{eff}}$ and $\xi$ from FeI
80404	7500	2.40	2.35	-0.14 $\pm$ 0.18 (26)	0.00 $\pm$ 0.06 (15)	H $\alpha$ and $\xi$ from FeII
90289	4100	1.70	1.49	+0.09 $\pm$ 0.16 (55)	+0.08 $\pm$ 0.15 (08)	$T_{\text{eff}}$ and $\xi$ from FeI
102839	4670	1.10	2.80	+0.11 $\pm$ 0.08 (30)	+0.11 $\pm$ 0.12 (10)	$T_{\text{eff}}$ and $\xi$ from FeI
114792	5600	2.35	7.44	+0.06 $\pm$ 0.17 (32)	+0.05 $\pm$ 0.07 (10)	H $\alpha$ and $\xi$ from FeII
159633	5200	1.85	4.45	+0.13 $\pm$ 0.09 (37)	+0.14 $\pm$ 0.06 (11)	H $\alpha$ and $\xi$ from FeII
192876	5300	2.20	3.18	+0.22 $\pm$ 0.08 (35)	+0.21 $\pm$ 0.06 (09)	H $\alpha$ and $\xi$ from FeII
204867	5700	2.05	4.29	+0.12 $\pm$ 0.10 (38)	+0.11 $\pm$ 0.13 (12)	H $\alpha$ and $\xi$ from FeII
225212	4100	0.75	2.95	+0.10 $\pm$ 0.20 (26)	+0.11 $\pm$ 0.22 (13)	$T_{\text{eff}}$ and $\xi$ from FeI

difference between the FeI and FeII means equalled the higher standard deviation. We consider that to be the  $1\sigma$  uncertainty in log g. All the uncertainties are listed in Table 4.

### 3.7. Comparison with the literature

Some of the stars analyzed in this work have atmospheric parameters that are published in the literature. Our determinations show an overall good agreement with them. Some values from the literature are listed in Table 5 along with ours for comparison. Most of these results are from high resolution spectroscopic analysis.

Out of our sample, Canopus (HD 45348) is probably the most extensively studied star. Among the published parameters, we believe the set by Jerzykiewicz & Molenda-Zacowicz (2000) to be the most reliable. In that work the temperature is derived from measurements of the angular diameter and the total absolute flux. The gravity is derived by placing the star in a theoretical evolutionary diagram using the above temperature and luminosity obtained from the Hipparcos parallax and the total flux.

Our temperature for Canopus is in excellent agreement with theirs, as well as with the others, as shown in Table 5. Our gravity is slightly higher but is also in agreement with theirs within the uncertainties. However it is important to stress that it is not possible to fit the observed H $\alpha$  wings with a temperature around 7500K and a smaller gravity than 2.10 dex. The other parameters also agree well with the values from the literature.

The picture is the same for the other stars as there is generally good agreement. However our gravity tends to be higher than previously determined, especially in the case of HD 80404. Again it is not possible to fit the observed H $\alpha$  wings for this star with a temperature around 7500K and a smaller gravity than 2.40 dex.

The only star for which the agreement is not good is HD 204867. Luck (1977) employed curves of growth to do his analysis. Foy (1981) reanalyzed the same star using equivalent widths but adopting the same temperature determined by Luck (1977). The interesting fact, however, is that both analyses made use of the models by Gustafsson et al. (1975). Thus the differences are mainly due to the different set of *gfs* employed. This shows the importance of well-determined *gfs*. It seems that our method of determining the temperature is more reliable and shows excellent agreement with the temperatures from the FeI and FeII excitation equilibria.

### 3.8. Masses

We also estimated the masses of our sample stars. To do so we placed the stars in the HR diagram with theoretical evolutionary tracks. Luminosities were calculated using  $M_V = V - A_V + 5 + 5\log \pi$  and the bolometric corrections from Alonso et al. (1999) and adopting a solar bolometric magnitude,  $M_{\text{Bol}\odot} = 4.75$  (Cram 1999),  $\log(L_*/L_\odot) = -0.4(M_{\text{Bol}*} - M_{\text{Bol}\odot})$ .

Once the stars are placed in the HR diagram their masses can be estimated by interpolating among the tracks. Some of the stars fall in regions where blue loops may occur, so they have two mass estimates, one for the first crossing and the second one for the blue loop. These masses are listed in Table 6. HD 1219 falls below the tracks, so its mass could not be estimated. Probably its parallax is wrong, leading to wrong distance and wrong reddening and luminosity. HD 90289 seems to be in the AGB region of the HR diagram.

Based on the uncertainties of the parallaxes, visual magnitudes, extinctions, and bolometric corrections, we estimate the mean uncertainty of  $\log(L_*/L_\odot)$  to be  $\approx 0.08$  dex. The mean uncertainty of  $\log(T_{\text{eff}})$  is  $\approx 0.01$  dex. There are, however, other sources of uncertainties, which we cannot estimate, affecting

**Table 5.** Atmospheric parameters available in the literature in comparison with the present results.

HD	$T_{\text{eff}}$	$\log g$	$\xi$	[Fe/H]	Ref.
45348	7500	2.10	3.30	-0.04	this work
45348	7464	1.68-1.76	-	-	(1)
45348	7575	1.90-2.10	3.00	-0.25	(2)
45348	7500	1.50	2.50	+0.06	(3)
45348	7500	1.20	3.00	+0.08	(4)
45348	7500	1.50	3.50	-0.07	(5)
36673	7450	1.90	4.70	0.00	this work
36673	7350	1.80	3.00	-0.05	(2)
36673	7400	1.50	5.90	-0.06	(6)
36673	7000	1.30	2.50	-0.10	(5)
80404	7500	2.40	2.35	-0.14	this work
80404	7500	1.60	2.20	+0.02	(7)
80404	7500	0.90	2.50	+0.06	(5)
49068	4625	2.20	1.78	+0.19	this work
49068	4500	2.00	2.00	0.00	(8)
204867	5700	2.05	4.29	+0.12	this work
204867	5362	1.15	3.50	-0.05	(9)
204867	5475	1.60	3.10	-0.02	(10)
204867	5475	1.30	2.30	+0.19	(11)
225212	4100	0.75	2.95	+0.10	this work
225212	4250	0.80	4.50	-0.20	(12)

(1) Jerzykiewicz & Molenda-Zacowicz 2000, (2) Luck et al. 1998, (3) Hill et al. 1995, (4) Spite et al. 1989, (5) Luck & Lambert 1985, (6) Venn 1995a, (7) Luck & Lambert 1985, (8) Gilroy 1989, (9) Luck 1982, (10) Foy 1981, (11) Luck 1977, (12) Luck & Bond 1980.

the luminosities. First, the evolutionary tracks we used are for solar metallicity stars, however, most of our sample stars are slightly more metallic than that. Second, the adopted tracks do not take rotation into account. Rotation is supposed to change not only the photospheric abundances but also the evolutionary path along the HR diagram.

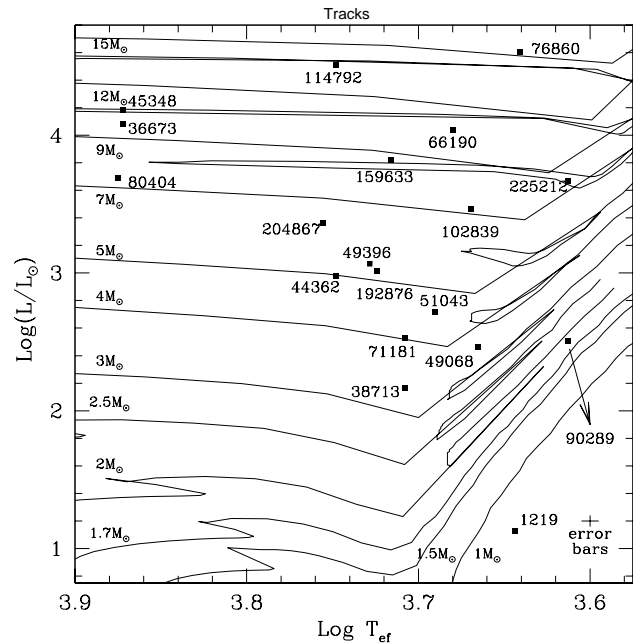
#### 4. Abundances

In this section we discuss the determination of CNO abundances. All the abundances were derived using spectral synthesis. The codes for calculating synthetic spectra are described by Barbuy et al. (2003). The adopted C, N, and O atomic lines are listed in Table 7 with corresponding excitation potential and oscillator strength.

##### 4.1. Carbon

Carbon abundances were calculated from the CI line  $\lambda 5380.322\text{\AA}$  for stars that are hotter than 5200K and from the C<sub>2</sub> lines at  $\lambda 5135.62\text{\AA}$  for cooler stars. The oscillator strength of the CI line,  $\log gf = -1.64$ , was derived by fitting the solar spectrum with the solar abundance recommended by Grevesse & Sauval (1998),  $A_C = 8.52$ . We used the solar spectrum available on the internet<sup>2</sup> observed with UVES at the VLT.

<sup>2</sup> The spectrum is freely available for download at the ESO website: [www.eso.org/observing/dfo/quality/UVES/pipeline/solar\\_spectrum.html](http://www.eso.org/observing/dfo/quality/UVES/pipeline/solar_spectrum.html)

**Fig. 2.** The HR diagram with our stars and the theoretical evolutionary tracks from Schaller et al. (1992).**Table 6.** The bolometric magnitudes, bolometric corrections, luminosities, and estimated masses.

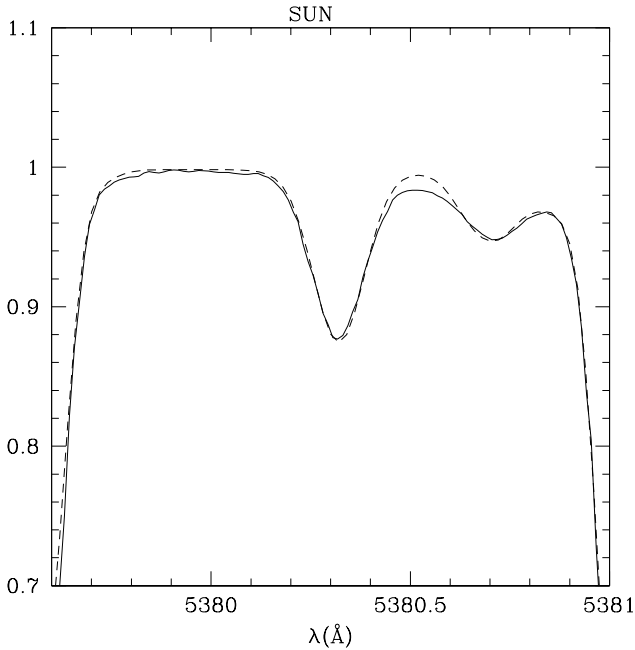
HD	$M_{\text{Bol}}$	BC	$\log(L_*/L_\odot)$	Mass in $M_\odot$
1219	1.94	-0.57	1.13	-
36673	-5.46	0.00	4.08	10.1 - 8.6
38713	-0.67	-0.23	2.17	3.4
44362	-2.70	-0.12	2.98	5.0
45348	-5.71	0.00	4.18	10.6 - 9.0
49068	-1.41	-0.42	2.46	3.5
49396	-2.92	-0.16	3.07	5.4
51043	-2.04	-0.30	2.72	4.6
66190	-5.34	-0.34	4.04	10.6 - 8.3
71181	-1.57	-0.23	2.53	4.0
76860	-6.77	-0.58	4.62	15.5
80404	-4.47	-0.01	3.69	7.4
90289	-1.52	-0.83	2.51	1.9
102839	-3.91	-0.39	3.46	7.3 - 6.0
114792	-6.53	-0.12	4.51	13.8 - 11.8
159633	-4.80	-0.20	3.82	8.8 - 7.0
192876	-2.79	-0.17	3.02	5.3
204867	-3.66	-0.10	3.37	6.5 - 6.0
225212	-4.42	-0.83	3.67	7.9 - 7.0

A blend of lines on the red side of the CI line was treated as a set of FeI lines following Spite et al. (1989). The solar model was constructed using the grids of Kurucz (1994) and the parameters  $T_{\text{eff}} = 5780\text{K}$ ,  $\log g = 4.44\text{dex}$ , and  $\xi = 1.00\text{km s}^{-1}$ . Figures 3 and 4 show the observed spectrum and the synthetic fits for the Sun and the star HD 36673.

The C<sub>2</sub>(0,0)  $\lambda 5135.62\text{\AA}$  is a band of the Swan system. The data of the C<sub>2</sub> molecule are those by Barbuy (1985), dissociation

**Table 7.** Data of the adopted C, N, and O atomic lines.

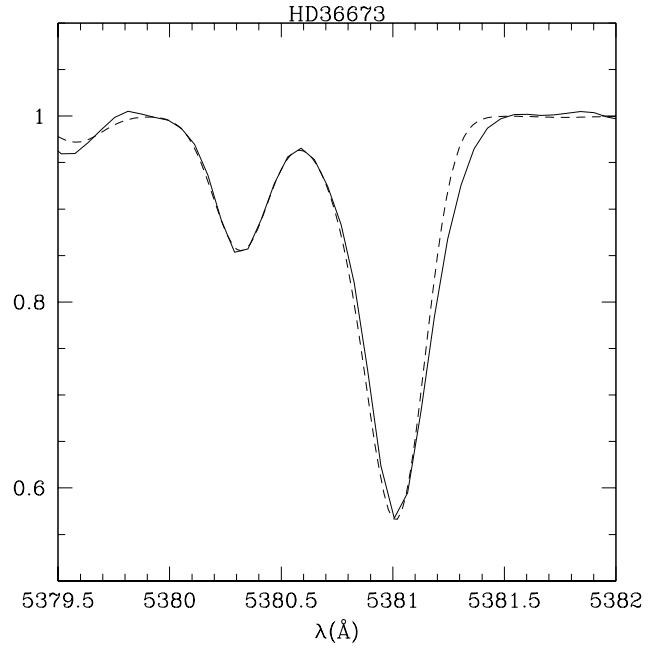
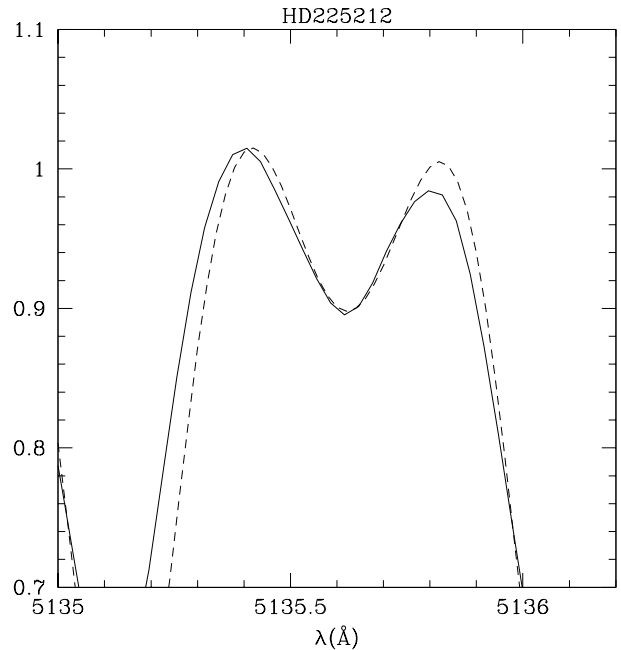
Species	$\lambda$ (Å)	$\chi$ (eV)	$\log gf$
CI	5380.322	7.68	-1.640
NI	7442.310	10.33	-0.385
NI	7468.312	10.33	-0.190
NI	8200.357	10.33	-1.001
NI	8210.715	10.33	-0.708
NI	8216.336	10.33	+0.132
NI	8242.389	10.33	-0.256
OI	6156.737	10.74	-1.487
OI	6156.755	10.74	-0.898
OI	6156.778	10.74	-0.694
OI	6158.149	10.74	-1.841
OI	6158.172	10.74	-0.995
OI	6158.187	10.74	-0.409
[OI]	6300.311	0.00	-9.716

**Fig. 3.** Fit to the CI  $\lambda 5380.320\text{\AA}$  line in the Sun. The synthetic spectrum (dashed) is compared to the observed one (solid).

tion potential  $D_0(\text{C}_2) = 6.21$  eV and electronic-vibrational oscillator strength  $f_{00} = 0.0184$ . An example of fit is shown in Fig. 5 for HD 225212.

Venn (1995a) analyzed the influence of NLTE effects in the carbon abundances derived from CI lines in a sample of A0-F0 supergiants. It was shown that NLTE is important, and the abundances derived by assuming ETL must be corrected. The amplitude of the correction increases from F0 type stars to A0 type.

Even though we do not have the means to estimate the exact correction that must be applied, we adopted a mean correction. Among the stars analyzed by Venn (1995a), HD 36673 is also in our sample. There are also two other stars with similar spectral type, HD 25291 (F0II) and HD 6130 (F0II). Venn's analysis has shown that the mean carbon abundances of these stars

**Fig. 4.** Fit to the CI  $\lambda 5380.320\text{\AA}$  line in HD 36673. The synthetic spectrum (dashed) is compared to the observed one (solid).**Fig. 5.** Fit to the  $\text{C}_2$   $\lambda 5135.62\text{\AA}$  line in HD 225212. The synthetic spectrum (dashed) is compared to the observed one (solid).

should be corrected by  $-0.25\text{dex}$  (HD 36673),  $-0.24\text{dex}$  (HD 25291), and  $-0.16\text{dex}$  (HD 6130). We adopted the mean value,  $-0.22\text{dex}$ , as the correction that must be applied to the carbon abundances in the stars HD 36673 (F0Ib) and HD 45348 (F0II).

The abundance of the star HD 80404 (A8Ib) also needs to be corrected. For a star with similar spectral type, HD 58585



(A8II), Venn (1995a) adopts a correction of  $-0.33$  dex. We adopted the same value for HD 80404. The carbon abundances (as well as the nitrogen and oxygen abundances) are listed in Table 9. The abundances listed have already been corrected for NLTE effects whenever necessary.

#### 4.2. Nitrogen

Nitrogen abundances were derived from atomic lines for hotter stars than 5200K and from CN molecular lines for the cooler stars. We used two atomic lines from the multiplet 3 around  $\lambda 7444\text{\AA}$  and four lines of the multiplet 2 around  $\lambda 8220\text{\AA}$ . The line list and the *gfs* are listed in Table 7. The adopted *gfs* are the ones recommended by NIST (Martin et al. 2002).

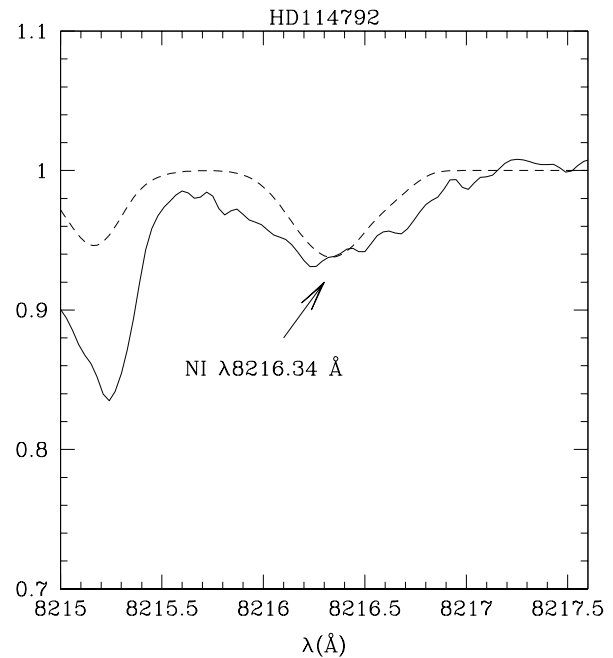
The CN lines we used are the CN(5,1)  $\lambda 6332.18\text{\AA}$  and CN(6,2)  $\lambda 6478.48\text{\AA}$  bandheads of the  $A^2\Pi-X^2\Sigma$  red system. The data of the CN lines are the same as adopted by Milone et al. (1992), dissociation potential  $D_0(\text{CN}) = 7.65$  eV and electronic oscillator strength  $f_{el} = 6.76 \cdot 10^{-3}$ . We adopted the solar abundance of nitrogen recommended by Grevesse & Sauval (1998),  $A_N = 7.92$ .

The region around  $\lambda 8220\text{\AA}$  is highly contaminated by telluric lines. In order to properly identify the telluric lines, we carefully compared the spectra of stars with distinct radial velocities. Any nitrogen line blended with a telluric one was excluded from the analysis. Since weak telluric lines may not be properly identified, some of the nitrogen lines may be slightly contaminated. Moreover, most of our stars are not hot enough to allow the high excitation atomic nitrogen lines to be well defined. They are also affected by some weak unidentified blends. Thus the synthetic fit for these lines should be considered with care, possibly as an upper limit for the abundance. Figure 6 exemplifies this situation.

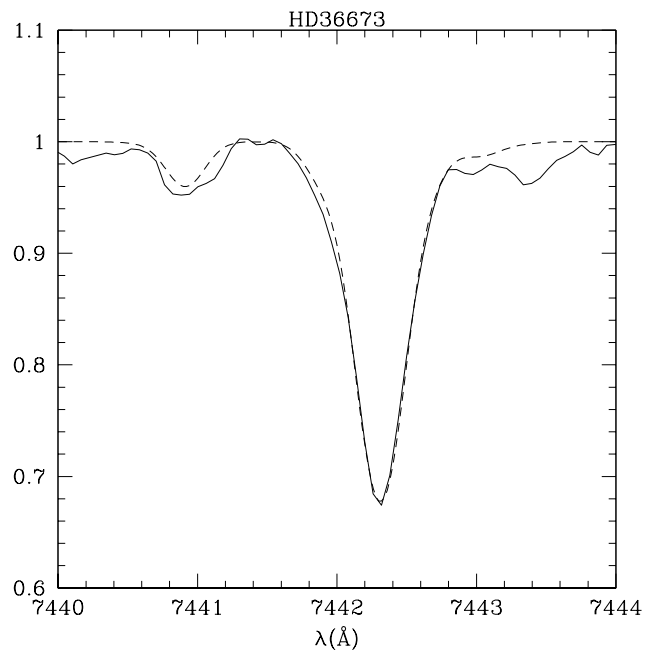
The two lines in the region around  $\lambda 7440\text{\AA}$  have no problem with telluric lines but are also affected by unidentified blends. We tried to simulate the blends with FeI lines for the three hottest stars. In these stars there are blends in both wings of both the adopted lines. These artificial lines did a good job in adjusting the line wings of the stars HD 36673 and HD 80404, but not as good for HD 45348, as shown in Figs. 7 and 8.

The molecular CN lines are also affected by blends. The band at  $\lambda 6332.18\text{\AA}$  is affected by two lines at  $\lambda 6331.95\text{\AA}$ , one due to SiI and the other due to FeII. Both are taken into account in the synthesis. In general the fit to this CN line is better than the fit to the  $\lambda 6478.48\text{\AA}$  line. Figures 9 and 10 are examples of the fits for the star HD 225212.

The nitrogen abundances of the stars HD 36673, HD 45348, and HD 80404 are affected by NLTE. Venn (1995a) investigated the effects of NLTE in the nitrogen abundances. In order to correct our results from NLTE effects, we proceeded as we did for carbon, by adopting mean corrections based on the results by Venn (1995a) for stars with similar spectral type to ours. Thus, the mean nitrogen abundances were corrected by  $-0.31$  dex for HD 36673 and HD 45348 and by  $-0.58$  dex for HD 80404. Table 8 lists the abundances derived from each line for each star. In this table the abundances have not been cor-



**Fig. 6.** Fit to the NI  $\lambda 8216.34\text{\AA}$  in HD 114792 line. The synthetic spectrum (dashed) is compared to the observed one (solid). This star has a temperature of about 5600K. The nitrogen line is weak and affected by many weak unidentified blends.

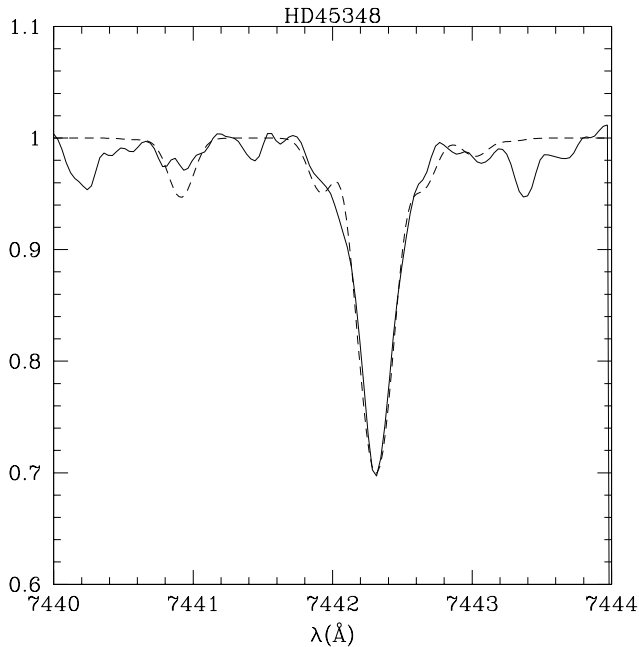
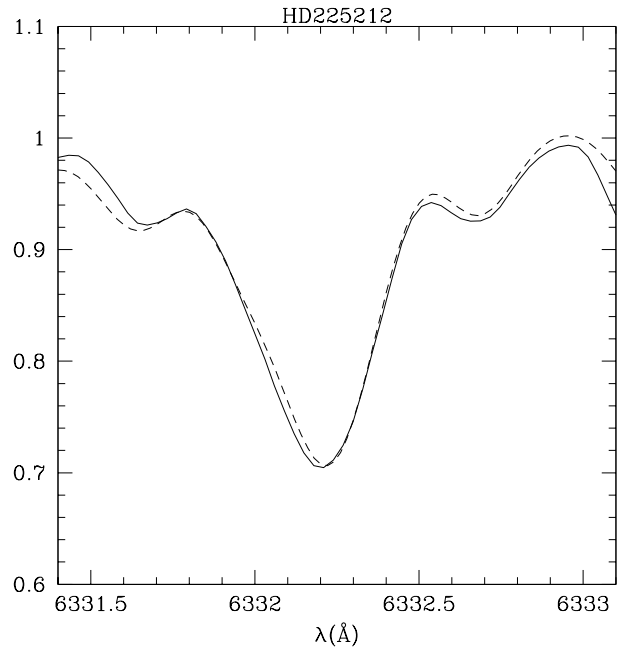


**Fig. 7.** Fit to the NI  $\lambda 7442.31\text{\AA}$  line in HD 36673. The synthetic spectrum (dashed) is compared to the observed one (solid).

rected for NLTE, the ones corrected for NLTE are listed in Table 9.

**Table 8.** The abundances of nitrogen line by line in each star. The abundances in this table are not corrected for NLTE.

HD	7442	7468	8200	8210	8216	8242	CN(5,1)	CN(6,2)
1219	–	–	–	–	–	–	8.07	7.92
36673	8.88	9.01	8.67	–	–	–	–	–
38713	–	–	–	–	–	–	8.27	–
44362	8.24	–	–	–	–	–	–	–
45348	8.60	8.72	–	8.60	–	–	–	–
49068	–	–	–	–	–	–	8.63	8.71
49396	8.74	–	–	–	–	–	–	–
51043	–	–	–	–	–	–	8.54	–
66190	–	–	–	–	–	–	9.01	9.15
71181	–	–	–	–	–	–	8.84	8.75
76860	–	–	–	–	–	–	8.92	8.80
80404	8.82	9.06	–	8.68	–	8.62	–	–
90289	–	–	–	–	–	–	–	–
102839	–	–	–	–	–	–	8.46	8.37
114792	8.30	8.27	–	–	8.19	8.46	–	–
159633	–	–	–	–	–	–	–	–
192876	8.66	–	–	–	–	–	–	–
204867	8.58	8.24	–	–	–	–	–	–
225212	–	–	–	–	–	–	8.47	8.39

**Fig. 8.** Fit to the Ni I  $\lambda 7442.31\text{\AA}$  line in HD 45348. The synthetic spectrum (dashed) is compared to the observed one (solid).**Fig. 9.** Fit to the CN band  $\lambda 6332.18\text{\AA}$  in HD 225212. The synthetic spectrum (dashed) is compared to the observed one (solid).

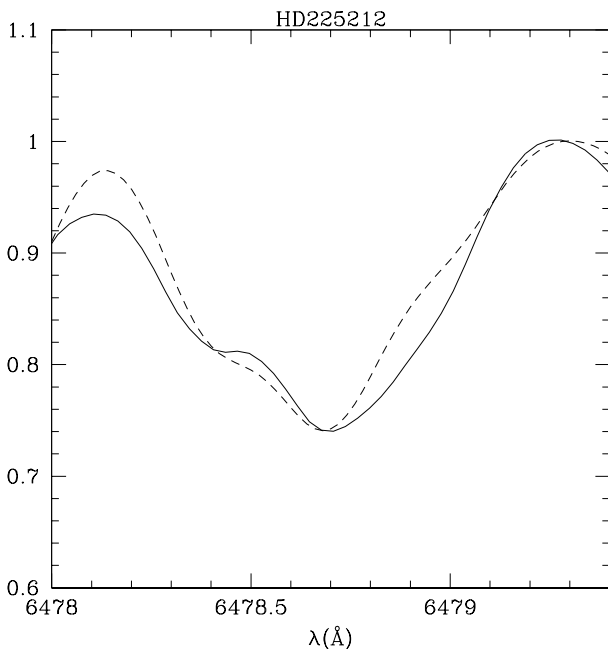
### 4.3. Oxygen

Oxygen abundances were calculated from two lines of the OI permitted triplet, at  $\lambda 6156.7\text{\AA}$  and  $\lambda 6158.1\text{\AA}$  for the three hottest stars, and from the [OI] forbidden line, at  $\lambda 6300.311\text{\AA}$  for the other stars. We adopted the recommended data for the fine structure of the permitted lines from NIST (Martin et al. 2002). The atomic data used are reported in Table 7. The solar abundance we adopted is the one suitable for the 1D models recommended by Allende Prieto et al. (2001),  $A_{\text{O}} = 8.77$ .

The forbidden line is blended with a weak NiI line at  $\lambda 6300.34\text{\AA}$ , which is included in the synthesis with parameters recommended by Allende Prieto et al. (2001). It also has a nearby ScII line at  $\lambda 6300.70\text{\AA}$  for which we adopted the hyperfine structure by Spite et al. (1989). In Figs. 11 and 12 we show examples of the fits for the forbidden line in HD 44362 and HD 159633, while Fig. 13 shows an example of the fit for the permitted lines in HD 80404.

**Table 10.** The uncertainties of the abundances.

HD	Elem.	Line	$\sigma_{Teff}$	$\sigma_{logg}$	$\sigma_{\xi}$	$\sigma_{[Fe/H]}$	$\sigma_{total}$
49396	C	$\lambda 5380.32\text{\AA}$	-0.09	+0.15	+0.05	-0.06	$\pm 0.19$
76860	C	$C_2 \lambda 5135.62\text{\AA}$	-0.05	+0.06	-0.01	-0.07	$\pm 0.11$
36673	N	$\lambda 7442.31\text{\AA}$	-0.02	+0.03	0.00	-0.16	$\pm 0.16$
36673	N	$\lambda 7468.31\text{\AA}$	0.00	+0.05	0.00	-0.16	$\pm 0.17$
36673	N	$\lambda 8200.36\text{\AA}$	-0.01	+0.04	0.00	-0.16	$\pm 0.17$
76860	N	$CN \lambda 6332.18\text{\AA}$	-0.04	+0.15	+0.02	-0.02	$\pm 0.16$
76860	N	$CN \lambda 6478.48\text{\AA}$	-0.08	+0.02	-0.06	-0.13	$\pm 0.17$
36673	O	$\lambda 6157\text{\AA}$	-0.03	+0.03	0.00	-0.17	$\pm 0.18$
49396	O	$\lambda 6300.31\text{\AA}$	+0.04	+0.11	0.00	-0.07	$\pm 0.14$
76860	O	$\lambda 6300.31\text{\AA}$	-0.01	+0.10	-0.01	-0.08	$\pm 0.13$

**Fig. 10.** Fit to the CN band  $\lambda 6478.48\text{\AA}$  in HD 225212. The synthetic spectrum (dashed) is compared to the observed one (solid).

According to Takeda & Takada-Hidai (1998), the oxygen abundances, as derived from the permitted triplet in  $\lambda 6156\text{\AA}$  for stars hotter than 5750K, are affected by NLTE. This temperature limit applies to HD 36673, HD 45348, and HD 80404. For stars with similar temperatures to ours, 7500K, Takeda & Takada-Hidai (1998) estimate a correction of about  $-0.15\text{dex}$ . We thus corrected our abundances by that amount. The oxygen abundances, corrected for NLTE whenever necessary, are listed in Table 9.

#### 4.4. Uncertainties of the abundances

The main source of uncertainties in the abundances are those in the determining the atmospheric parameters. In order to estimate the uncertainties in the abundances, we changed each atmospheric parameter by its uncertainty, keeping the other ones with the original adopted values, and recalculated the abun-

**Table 9.** Abundances of C, N, and O.

HD	[C/Fe]	[N/Fe]	[O/Fe]
1219	0.00	-0.12	-
36673	-0.86	+0.62	-0.25
38713	-0.14	+0.30	-0.14
44362	-	+0.22	-0.31
45348	-0.55	+0.45	-0.11
49068	-0.23	+0.56	+0.06
49396	-0.61	+0.68	+0.10
51043	-0.19	+0.60	-0.07
66190	-0.39	+0.90	0.00
71181	-0.23	+0.74	+0.09
76860	-0.24	+0.77	+0.13
80404	-0.55	+0.44	+0.08
90289	-0.13	-	+0.13
102839	-0.26	+0.39	-0.13
114792	-0.49	+0.33	+0.14
159633	-	-	+0.06
192876	-0.61	+0.52	-0.01
204867	-0.63	+0.37	-0.06
225212	-0.14	+0.41	-0.02

dances. In this way one measures the effect of the parameter uncertainty in the abundance. Assuming that the effects of the uncertainties of the parameters are independent, we can calculate the total uncertainty,  $\sigma_{total}$ ,

$$\sigma_{total} = \sqrt{(\sigma_{Teff})^2 + (\sigma_{logg})^2 + (\sigma_{\xi})^2 + (\sigma_{[Fe/H]})^2}, \quad (1)$$

the results are listed in Table 10.

Since we used the stars HD 49396 and HD 76860 to estimate the uncertainties in the parameters, the obvious choice was to choose them to estimate the uncertainties in the abundances. However the nitrogen abundance in the star HD 49396 was estimated with only one line, and that line has the same problems as were discussed above and exemplified in Fig. 6 for HD 44362. We then chose another star in order to estimate the uncertainties in the nitrogen abundances, HD 36673. We also estimated the uncertainty in the oxygen abundance as derived from the permitted lines using HD 36673, since for both HD 49396 and HD 76860, the oxygen abundance was derived from the forbidden line. As can be noted in Table 10,  $\sigma_{total}$  is always less than  $\pm 0.20\text{dex}$ .

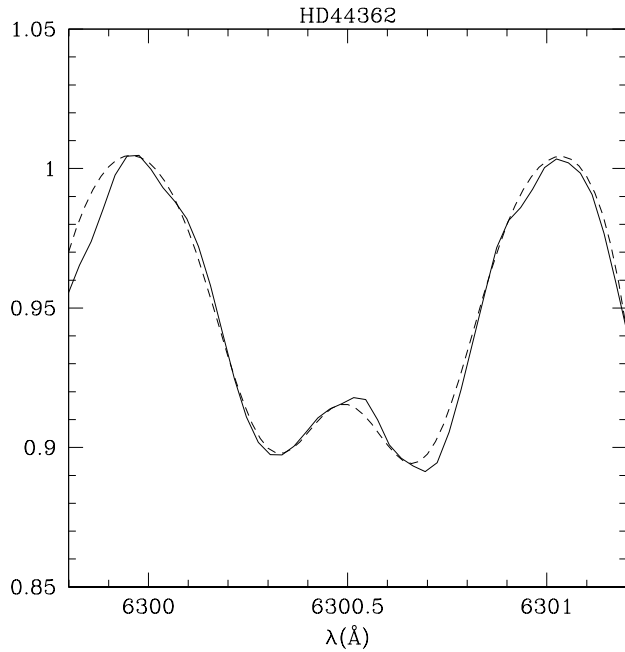


**Fig. 11.** Fit to the [OI]  $\lambda 6300.311\text{\AA}$  line in HD 44362. The synthetic spectrum (dashed) is compared to the observed one (solid).

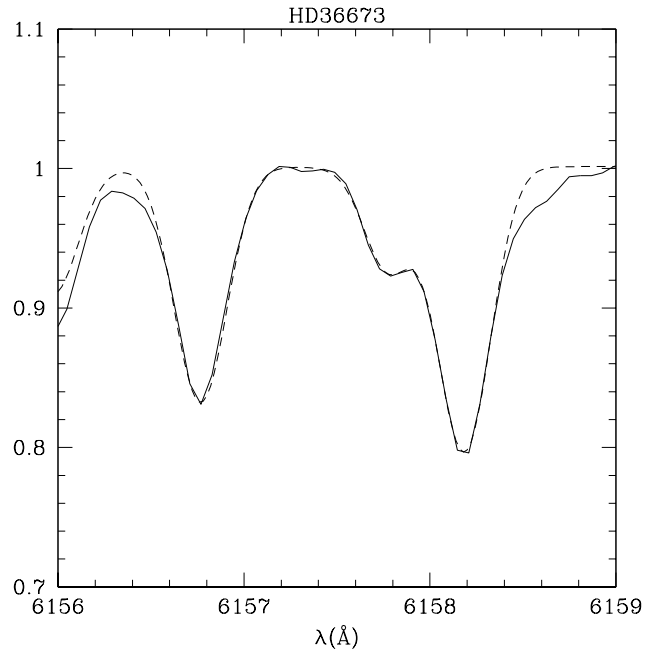


**Fig. 13.** Fit to the OI  $\lambda 6156.7\text{\AA}$  and  $\lambda 6158.1\text{\AA}$  lines in HD 36673. The synthetic spectrum (dashed) is compared to the observed one (solid).

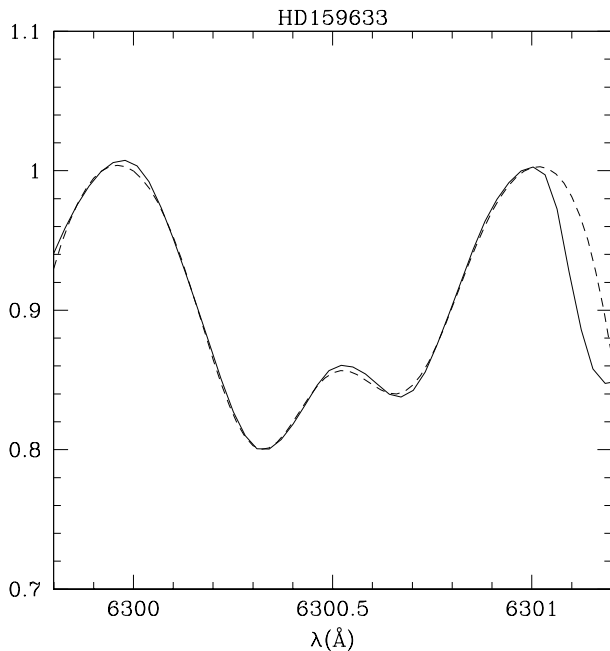


**Fig. 12.** Fit to the [OI]  $\lambda 6300.311\text{\AA}$  line in HD 159633. The synthetic spectrum (dashed) is compared to the observed one (solid).

## 5. Discussion

In order to discuss the evolutionary status of the stars, in particular whether the first dredge-up has already happened, it is more appropriate to use the ratio  $[N/C]$  rather than solely the N or C abundances. This ratio is listed in Table 11 together with the sum of the C, N, and O abundances. We exclude HD

1219 in the forthcoming discussion since we were not able to estimate its mass.

The mean  $[N/C]$  ratio for the sample stars is  $[N/C] = +0.95 \pm 0.28$ . The high value of the standard deviation is due to the high spread among the  $[N/C]$  values. The post first dredge-up prediction of Schaller et al. (1992) is approximately  $[N/C] = +0.60$  for stars between 2 and  $15 M_{\odot}$ , with smaller variations than 0.05 dex.

Meynet & Maeder (2000) calculate evolutionary models with an initial rotation velocity of  $300 \text{ km s}^{-1}$  for 9- $120 M_{\odot}$  stars. They also calculate non-rotating models in the same range of mass using the same input physics (opacities, nuclear rates, etc.). For the non-rotating models only the one with  $9 M_{\odot}$  develops a blue loop. In the rotating models, the  $12 M_{\odot}$  one also has a blue loop.

For the  $9 M_{\odot}$ , Meynet & Maeder (2000) predict  $[N/C] = +0.72$  without rotation and  $[N/C] = +1.15$  with rotation in the blue supergiant phase, after the dredge-up and during the blue loop. In the case of the  $12 M_{\odot}$  model without rotation, no change is predicted in the abundances. This model has no blue loop, thus a blue supergiant with this mass is only predicted to be crossing the HR diagram before the dredge-up. The  $12 M_{\odot}$  model with rotation is predicted to have  $[N/C] = +1.24$ . Less massive models are not calculated. However, it is probably reasonable to assume that the non-rotating less massive models, as well as the  $12 M_{\odot}$  model, would show similar abundances to the  $9 M_{\odot}$  model,  $[N/C] = +0.72$ , after the first dredge-up.

Adopting a tolerance of  $\pm 0.20 \text{ dex}$ ,  $[N/C]$  ratios between  $+0.52$  and  $+0.92$  would be in agreement with the Meynet & Maeder (2000) results for non-rotating stars. This means that no extra mixing process is needed to explain the abundances observed in the stars HD 49068, HD 51043, HD 102839, HD

**Table 11.** [N/C] ratio and the sums C+O, C+N, and C+N+O.

HD	[N/C]	C+N	C+O	C+N+O
1219	-0.12	8.79	—	—
36673	+1.48	8.59	8.55	8.85
38713	+0.44	8.66	8.87	8.97
44362	—	—	—	—
45348	+1.00	8.48	8.68	8.84
49068	+0.79	8.88	8.87	9.08
49396	+1.29	8.82	9.06	9.23
51043	+0.79	8.76	8.87	9.04
66190	+1.29	9.16	9.12	9.40
71181	+0.97	8.95	9.10	9.28
76860	+1.01	9.00	9.16	9.34
80404	+0.99	8.37	8.76	8.87
90289	—	—	9.11	—
102839	+0.65	8.70	8.90	9.03
114792	+0.82	8.51	9.02	9.10
159633	—	—	—	—
192876	+1.13	8.77	9.04	9.19
204867	+1.00	8.56	8.89	9.01
225212	+0.55	8.76	9.00	9.11

114792, and HD 225212. Their positions in the HR diagram (Fig. 2) seem to indicate that they are post first dredge-up stars. HD 114792 is definitely along a blue loop as is probably HD 102839.

The same argument could be used to argue that HD 38713 would not have passed through the first dredge-up, although its abundances are definitely altered. Thus, only an earlier mixing episode could be responsible for its abundances. However, if the same  $\pm 0.20$  dex tolerance is adopted for the Schaller et al. (1992) results, the [N/C] ratio of HD 38713 would be in marginal agreement with the predictions. Thus, we cannot be completely sure of its status.

There are four stars, HD 36673, HD 49396, HD 66190, and HD 192876, with [N/C] higher than +1.10 dex. These abundances cannot be explained by the non-rotating models. HD 36673 and HD 66190 are in blue loops. Their masses are around  $8.5M_{\odot}$  but they seem to be more mixed than predicted for the  $9M_{\odot}$  rotating model, especially HD 36673.

The abundances in HD 49396 and HD 192876 are a little more difficult to understand. In the HR diagram (Fig. 2), they are placed where changed abundances would not be expected. The predicted blue loops for these lower masses do not extend this far.

Uncertainties in the abundances alone cannot explain this picture. In order to be unmixed stars, the [N/C] would need to be wrong by more than 1.0 dex. It is very unlikely for this to be the case. Even though we consider these abundances to be highly uncertain, they at least indicate the stars are fully mixed and thus they are probably post first dredge-up stars.

If we consider the effective temperatures and luminosities to be right, only a more extended blue loop for these low masses would reconcile the tracks and the abundances. A  $T_{\text{eff}}$  that is reduced by its uncertainty, 200K, would not bring the results to any agreement. However, the problem could lie in the luminosities.

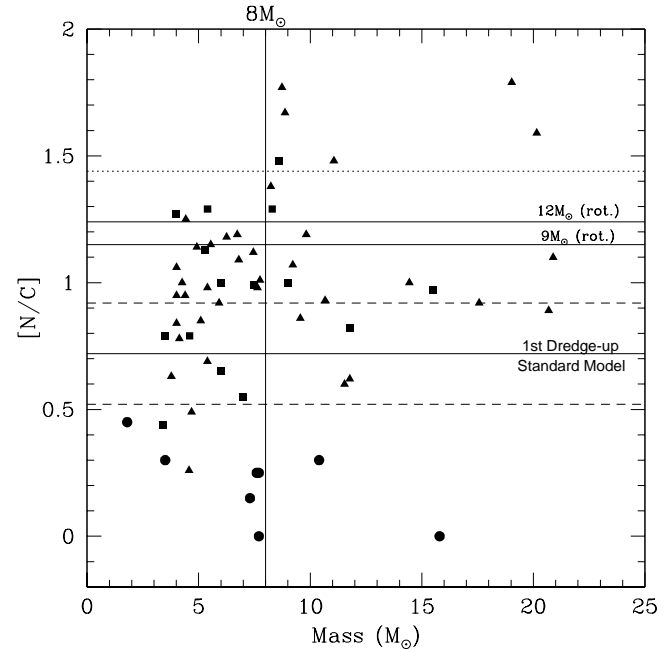


**Fig. 14.** Plot of the [N/C] ratio vs. the mass of the stars. The circles are stars from Barbuy et al. (1996), the triangles are stars from Luck & Lambert (1985), and the squares are the stars from this work. The solid horizontal lines represent the predictions for [N/C] after the 1st dredge-up from Meynet & Maeder (2000) for stars without rotation and for stars of  $9M_{\odot}$  and  $12M_{\odot}$  with initial rotation of  $300\text{km s}^{-1}$ , as indicated. The dashed lines represent the prediction without rotation  $\pm 0.2$  dex. The stars within these lines are considered to be fully mixed and in accordance with the non-rotating model. The dotted line represents the prediction of the  $12M_{\odot}$  rotating model  $+0.2$  dex.

As discussed before, at least for one star, HD 114792, we had a clear indication of problems with the  $A_V$  calculated from the work of Hakkila et al. (1997). For both HD 49396 and HD 192876, we also adopted  $A_V$  from that work. However, whereas for HD 114792 it seemed to be too high, for HD 49396 and HD 192876 it could be too low.

For both stars the photometric temperatures are smaller than the temperatures deduced from  $H\alpha$ . This would indicate that the reddening correction is underestimated. An increase in  $A_V$  would cause the stars to have a higher photometric temperature and higher luminosity. A higher luminosity is just what is needed to reconcile the position of the stars in the HR diagram to the blue loops of slightly more massive stars. However if one calculates the  $A_V$  needed to bring the temperatures into agreement, we see that it is not sufficient to cause an appreciable change in the luminosity. We are thus led to believe these stars are post first dredge-up stars in possibly more extended blue loops.

We still have the stars HD 45348, HD 71181, HD 76860, HD 80404, and HD 204867. All of them have [N/C] ratios that are only slightly higher than the limit of +0.92 dex, for which we would consider [N/C] to be in agreement with the non-rotating models. Since the predictions of the Meynet & Maeder (2000) models are for stars with a limiting high rotation ( $v =$

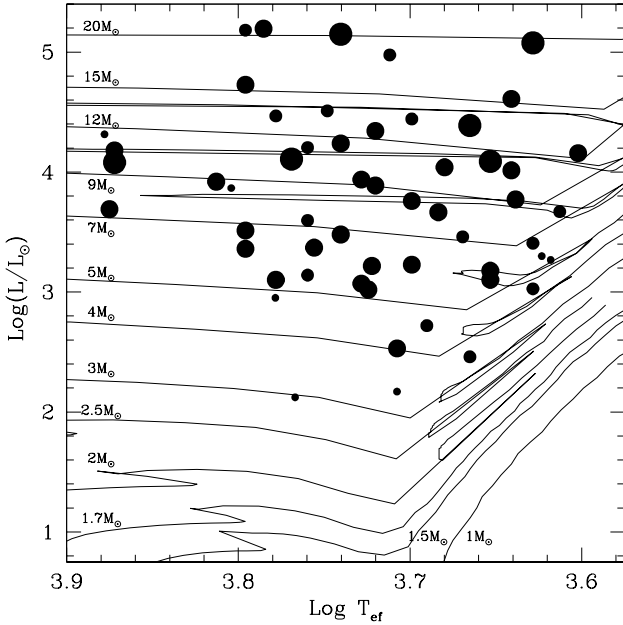


**Fig. 15.** HR diagram with the stars from this work, from Luck & Lambert (1985) and from Barbuy et al. (1996) divided according to their abundances. The stars are represented by circles with sizes that are proportional to the  $[N/C]$  ratio. The smaller circles are the stars with  $[N/C] < +0.52$ , the second smaller are stars with  $+0.52 < [N/C] < +0.92$ , the second larger the ones with  $+0.92 < [N/C] < +1.44$ , and the larger ones the stars with  $[N/C] > 1.44$ . The evolutionary tracks are the ones by Schaller et al. (1992).

$300 \text{ km s}^{-1}$ ), the abundances of these stars would be in agreement with a mixing induced by a lower rotation. Although these abundances seem to indicate more efficient mixing, we have to keep in mind that the uncertainties of the abundances do not allow a firm conclusion.

Figure 14 is a plot of the  $[N/C]$  ratio vs. stellar mass with the stars of our sample, of the sample analyzed by Luck & Lambert (1985) and of the sample by Barbuy et al. (1996). Masses for the stars of Luck & Lambert (1985) were estimated as in Barbuy et al. (1996) with the mass-luminosity relation by Schaller et al. (1992). As for our sample we can see the existence of stars spanning a variety of mixing efficiencies. There are stars only partially mixed, stars fully mixed and in agreement with the non-rotating model, stars fully mixed, but beyond what is predicted by the standard model, that can in principle be explained by the rotating models. We can also identify a fourth group of stars that seem to be mixed beyond what is predicted by the rotating models.

In Fig. 14 only stars that are more massive than about  $8M_{\odot}$  seem to be more mixed than expected for the rotating models. We can also note some  $5M_{\odot}$  stars that are mixed as predicted for the  $12M_{\odot}$  stars. These indicate that, although the rotation-induced mixing included in the models can produce  $[N/C]$  ratios compatible with the observations, there are details in the mass dependence of the results yet to be explored. Of course

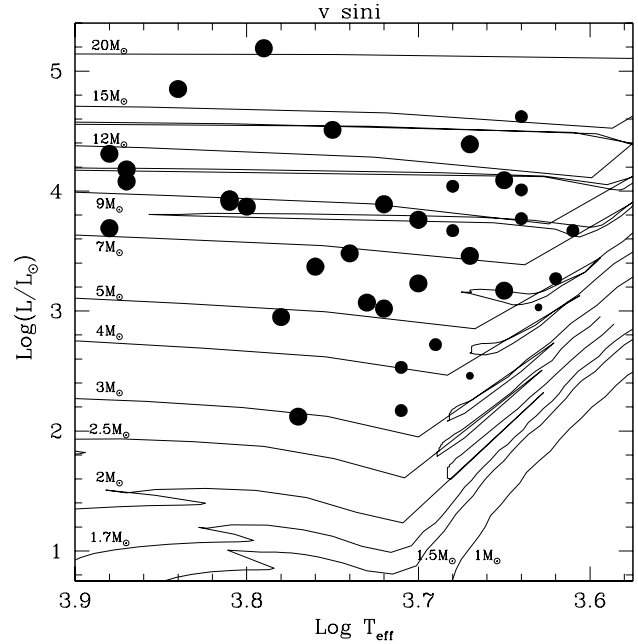


**Fig. 16.** HR diagram with the stars from this work, from Luck & Lambert (1985) and from Barbuy et al. (1996) divided according to their  $v \sin i$ . The stars are represented as circles proportional to the  $v \sin i$ . The smaller circles are stars with  $v \sin i < 2.00 \text{ km s}^{-1}$ , the medium size circles are the stars with  $2.00 \text{ km s}^{-1} < v \sin i < 6.00 \text{ km s}^{-1}$ , and the larger ones are stars with  $v \sin i > 6.00 \text{ km s}^{-1}$ .

this should be seen with caution since accurately determining stellar masses is not an easy matter.

Figure 15 shows the distribution along the HR diagram of the same stars plotted in Fig. 14. This time, however, the stars are divided in four groups according to their abundances. We note that the different group of stars overlap, which is not difficult to understand since the blue loops occur in this region of the HR diagram. However we also note a group of fully mixed stars with masses around  $5M_{\odot}$  again in a region where blue loops are not expected. We cannot state whether this is due to an incorrect estimation of the masses or to an underestimated extent of the blue loops.

Figure 16 shows the distribution along the HR diagram only for the stars for which  $v \sin i$  have been determined in the literature. The stars are again represented as circles, this time with sizes proportional to their  $v \sin i$ . Very interesting to note is that in Fig. 16 the stars with smaller  $v \sin i$  tend to be concentrated towards the right side of the HR diagram. This is an expected result, since the  $v \sin i$  is expected to decrease with increasing radii, and lower  $T_{\text{eff}}$ , during the evolution of the star. The observed  $v \sin i$  thus is not the initial  $v \sin i$  that would drive the mixing in the main sequence.

The  $[N/C]$  values depend both on the stellar mass and on its initial  $v \sin i$ . In order to try to disentangle the various effects, we plotted  $[N/C]$  vs. mass in intervals of temperature representing the stars again as circles with sizes proportional to  $v \sin i$  (Fig. 17). Some hints of trends can readily be seen, but in none of the plots are the trends strong. However, when considering the

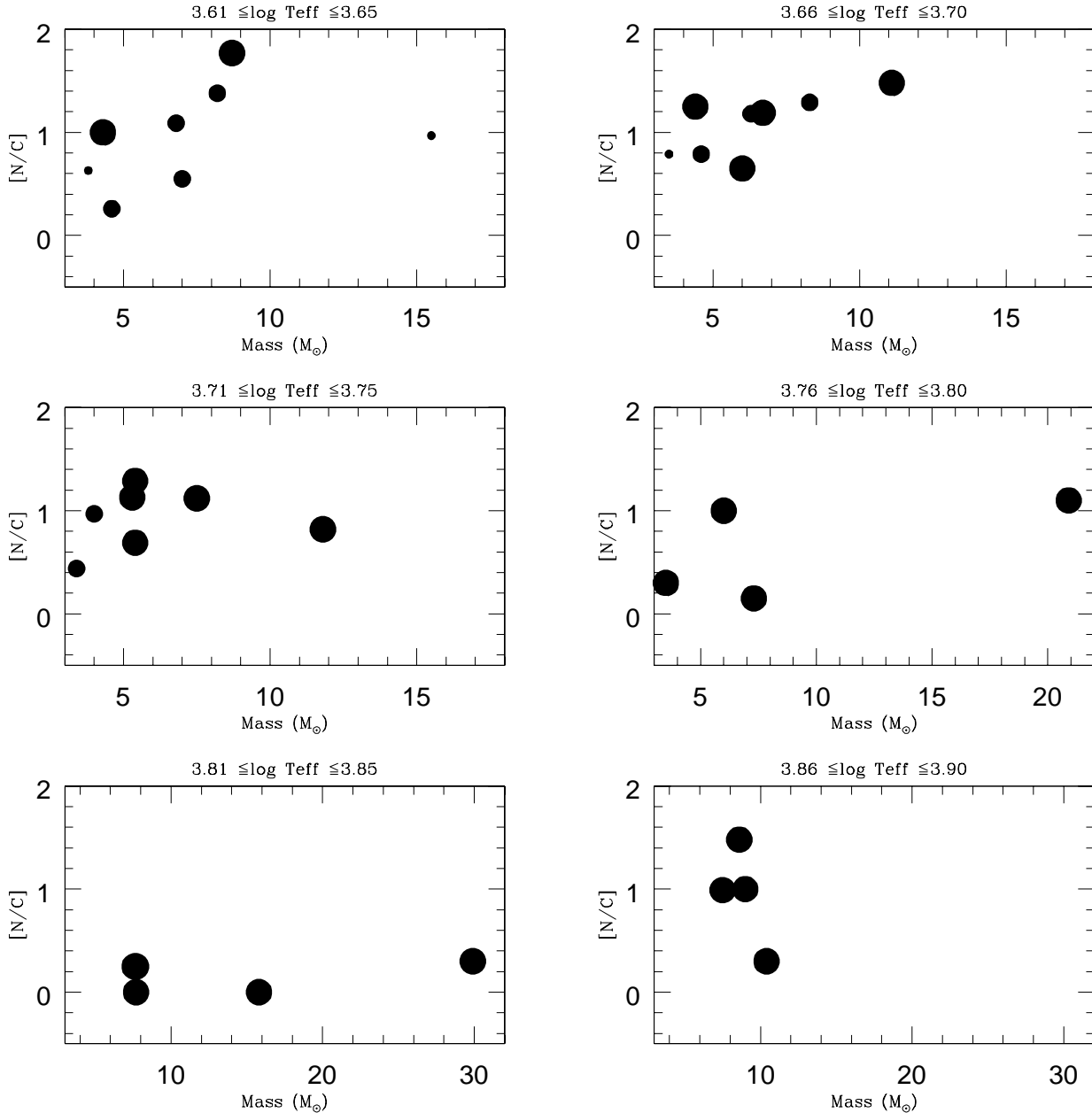


**Fig. 17.** [N/C] vs. stellar mass divided in intervals of temperature. The symbols are related to the  $v_{\text{cini}}$  in the same manner as in the last plot.

interval between  $\log T_{\text{eff}} = 3.61$  and  $\log T_{\text{eff}} = 3.70$ , the red supergiants, and only the stars with  $v_{\text{cini}} > 6 \text{ km s}^{-1}$  an important correlation can be seen (Fig 18). This correlation indicates a large increase in [N/C] with increasing mass.

It is the first time that such a relation is obtained and it may represent a new and important constraint. One has to still keep in mind that the correlation is defined by only a small number of points and that there seems to be a large scatter. The scatter, however, is probably mostly due to the fact that a large number of the stars will reach the giant branch with  $v_{\text{cini}} > 6 \text{ km s}^{-1}$  and not only to observational uncertainties. Further work in extending the sample and confirming the correlation and the scatter is still needed.

As a last point, we recall that Luck & Lambert (1985) analyzed a sample of variable and non-variable cool supergiants and noted a correlation between the carbon and oxygen abundances of their sample stars. Based on this correlation, they argued that the dredge-up could possibly reach deeper regions where the action of the ON cycle would be important for the final abundances. In order to investigate this suggested correlation, we made a plot of carbon vs. oxygen for our sample (Fig. 19). There is no indication of correlation. Hence, there seems to be no need of any deep mixing to explain the abundances.

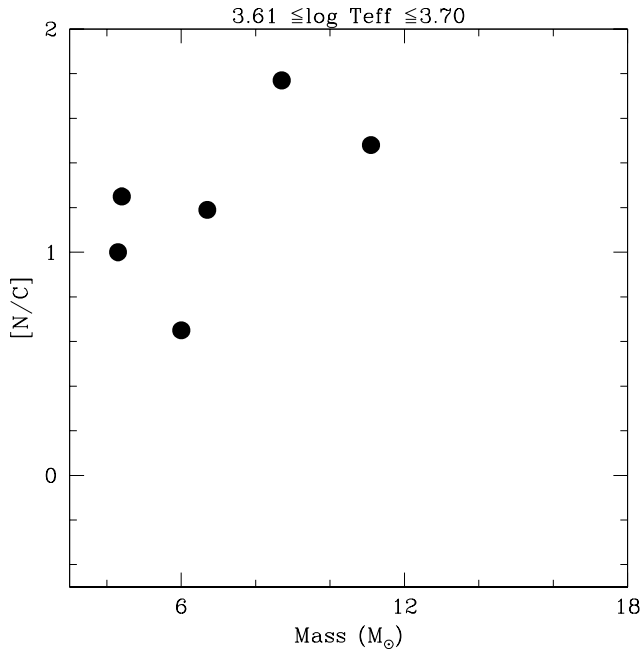


**Fig. 18.** Plot of [N/C] vs. stellar mass in the interval between  $\log T_{\text{eff}} = 3.61$  and  $\log T_{\text{eff}} = 3.70$  where a clear correlation can be noted. In this figure only the stars with  $v \sin i > 6 \text{ km s}^{-1}$  are plotted.

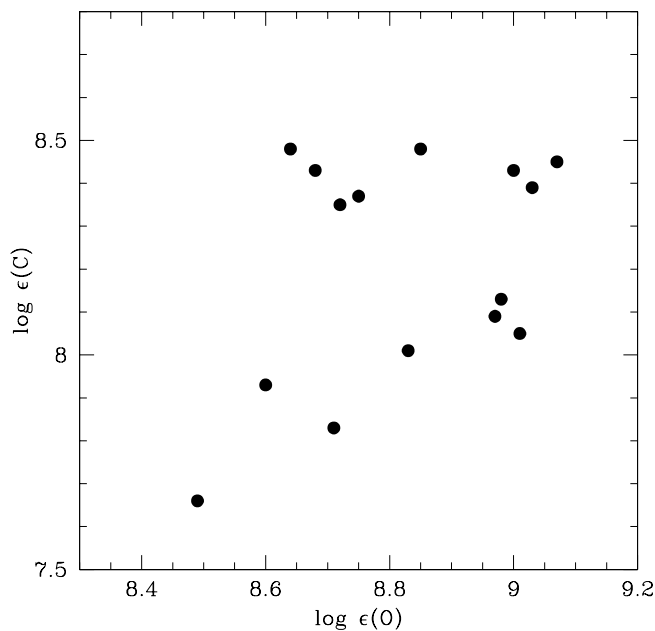


**Fig. 19.** Plot of the oxygen abundance vs. the carbon abundance. There is no correlation between them.

## 6. Conclusions

We carried out a detailed analysis of a sample of 19 evolved intermediate mass stars using high resolution spectra. We have determined atmospheric parameters, masses, and CNO abundances using spectral synthesis. Fifteen stars for which we were

able to determine both carbon and nitrogen show signs of internal mixing. The mean [N/C] ratio found is  $[N/C] = +0.95\text{dex}$ .

Only five of these stars, HD 49068, HD 51043, HD 102839, HD 114792, and HD 225212, have abundances in agreement with the predictions of non-rotating models by Meynet & Maeder (2000), which predict  $[N/C] = +0.72\text{dex}$ . One other star, HD 38713, would be less mixed than this but agrees marginally with the predictions of non-rotating models by Schaller et al. (1992),  $[N/C] = +0.60\text{dex}$ .

All the other stars show signs of a more efficient mixing process, i.e., [N/C] ratios higher than expected. The rotating models by Meynet & Maeder (2000) seem to show better agreement with the observed abundances. There seems to be, however, somewhat poor agreement when we consider the run of the abundances with the stellar mass, a point that needs further investigation.

Five of our stars, HD 45348, HD 71181, HD 76860, HD 80404, and HD 204867, have  $[N/C] \approx +1.0\text{dex}$ , less than what is predicted from rotating models with  $v = 300 \text{ km s}^{-1}$ . Thus, these stars might have lower rotation. Two other stars, HD 36673 and HD 66190, seem to have even higher [N/C] than predicted by these models. All this clearly indicates that the recent efforts to introduce rotation effects in the evolutionary models are producing results that are more compatible with observations.

The distribution of the stars in the HR diagram (Fig. 15) seems to indicate that the extension of the blue loops is underestimated at least in the  $5M_{\odot}$  track, further consideration of the uncertainties affecting the masses and luminosities of the stars in this region is needed before a firm conclusion can be drawn.

A correlation between [N/C] and stellar mass in the interval between  $\log T_{\text{eff}} = 3.61$  and  $\log T_{\text{eff}} = 3.70$  has been identified for the first time. This might represent an important constraint for the efforts at including rotation in the models. The correlation, however, is defined by a small number of points and should be investigated further.

We would like to emphasize that more observations are still needed. The CNO abundances, along with other elements that are affected by mixing processes such as Na and Li, must be determined in extended samples of A, F, G, K, and M evolved stars with low and high  $v \sin i$ . Only in this way will we be able to trace the mixing processes along the HR diagram and to better constrain the influence of rotation in the evolutionary models.

*Acknowledgements.* RS acknowledges a CAPES fellowship during the development of this work based on his MSc thesis. BB acknowledges grants from the Instituto do Milênio - CNPq, 620053/2001-1 and the FAPESP. JRM acknowledges financial support from the Instituto do Milênio - CNPq, 620053/2001-1 and the FAPERN Agency. The FEROS observations at the European Southern Observatory (ESO) were carried out within the Observatório Nacional ON/ESO and ON/IAG agreements, under Fapesp project n° 1998/10138-8.

## References

Allende Prieto, C., Lambert, D.L., Asplund, M., 2001, ApJ, 556, L63.  
Alonso, A., Arribas, S., Martinez-Roger, C., 1998, A&AS, 131, 209.



- Alonso, A., Arribas, S., Martínez-Roger, C., 1999, *A&AS*, 140, 261.
- Andrievsky, S.M., Kovtyukh, V.V., Usenko, I.A., 1996, *A&A*, 305, 551.
- Andrievsky, S.M., Kovtyukh, V.V., Luck, R.E., Lépine, J.R.D., Maciel, W.J., Beletsky, Yu. V., 2002, *A&A*, 392, 491.
- Andrievsky, S.M., Luck, R.E., Martin, P., Lépine, J.R.D., 2004, *A&A*, 413, 159.
- Arellano Ferro, A., Parrao, L., 1990, *A&A*, 239, 205.
- Boyarchuk, A.A., Lyubimkov, L.S., 1983, *Izv. Krym. Astrofiz. Obs.*, 66, 130.
- Barbuy, B., 1985, *A&A*, 151, 189.
- Barbuy, B., De Medeiros, J.R., Maeder, A., 1996, *A&A*, 305, 911.
- Barbuy, B., Perrin, M.N., Katz, D., Coelho, P., Cayrel, R., Spite, M., Van't Veer-Menneret, C., 2003, *A&A*, 404, 661.
- Castilho, B.V., Pasquini, L., Allen, D.M., Barbuy, B., Molaro, P., 2000, *A&A*, 361, 92.
- Chen, B., Vergely, J.L., Valette, B., Carraro, G., 1998, *A&A*, 336, 137.
- Cram, L., 1999, *Trans. IAU XXIII B*, 1999, 141, Editor: Andersen, J.
- Cutri, R.M. et al., 2003, *The 2Mass All-Sky Catalogue of Point Sources*, University of Massachusetts and Infrared Processing and Analysis Center (IPAC/California Institute of Technology)
- De Medeiros, J.R., Udry, S., Burki, G., Mayor, M. 2002, *A&A*, 395, 97.
- El Eid, M.F., Champagne, A.E., 1995, *ApJ*, 451, 298.
- ESA, 1997, *The Hipparcos and Tycho catalogues*, ESA SP-1200.
- Fliegner, J., Langer, N., Venn, K., 1996, *A&AL*, 308, 13.
- Foy, R., 1981, *A&A*, 103, 135.
- Gies, D., Lambert, D., 1992, *ApJ*, 387, 673.
- Gilroy, K., 1989, *ApJ*, 347, 835.
- Grevesse, N., Sauval, A.J., 1998, *Space Sci. Rev.*, 85, 161.
- Gustafsson, B., Bell, R., Eriksson, K., Nordlund, A., 1975, *A&A*, 43, 407.
- Hakkila, J., Myers, J.M., Stidham, B.J., 1997, *AJ*, 114, 2043.
- Hill, V., Andrievsky, S., Spite, M., 1995, *A&A*, 293, 347.
- Houdashelt, M.L., Bell, R.A., Sweigart, A.V., 2000, *AJ*, 119, 1448.
- Jerzykiewicz, M., Molenda-Zacowicz, J., 2000, *AcA*, 50, 369.
- Kaufer, A., Stahl, O., Tubbesing, S., Norregaard, P., Avila, G., Francois, P., Pasquini, L., Pizzella, A., 2000, *Performance report on FEROS, the new fiber-linked echelle spectrograph at the ESO 1.52-m telescope*, Proc. SPIE Vol. 4008, Optical and IR Telescope Instrumentation and Detectors, Masanori Iye; Alan F. Moorwood; Eds., 459.
- Kovtyukh, V.V., Andrievsky, S.M., Usenko, I.A., Klochkova, V.G., 1996, *A&A*, 316, 155.
- Kovtyukh, V.V., Andrievsky, S.M., 1999, *A&A*, 351, 597.
- Kurucz, R.L., 1994, CD-ROM 19.
- Lennon, D., Dufton, P., Mazzali, P., Pasian, F., Marconi, G., 1996, *A&A*, 314, 243.
- Luck, R.E., Gieren, W.P., Andrievsky, S.M., Kovtyukh, V.V., Fouqué, P., Pont, F., Kienzle, F., 2003, *A&A*, 401, 939.
- Luck, R.E., 1977, *ApJ*, 218, 752.
- Luck, R.E., 1982, *ApJ*, 256, 177.
- Luck, R.E., Bond, H., 1980, *ApJ*, 241, 218.
- Luck, R.E., Lambert, D.L., 1985, *ApJ*, 298, 782.
- Luck, R.E., Lambert, D.L., 1992, *ApJS*, 79, 303.
- Luck, R.E., Moffet, T., Barbes III, T., Gieren, W., 1998, *AJ*, 115, 605.
- Lyubimkov, L., 1998, *Astr. Rep.*, 387, 673.
- Lyubimkov, L., Boyarchuk, A.A., 1983, *Astrofizika*, 19, 683.
- Maeder, A., 1997, *A&A*, 321, 134.
- Maeder, A., Zahn, J.P., 1998, *A&A*, 334, 1000.
- Maeder, A., Meynet, G., 2000, *ARA&A*, 38, 143.
- Martin, W.C., Fuhr, J.R., Kelleher, D.E., et al. 2002, NIST Atomic Database (version 2.0), <http://physics.nist.gov/asd>. National Institute of Standards and Technology, Gaithersburg, MD.
- Mathis, S., Palacios, A., Zahn, J.P., 2004, *A&A*, 425, 243.
- Mathis, S., Zahn, J.P., 2004, *A&A*, 425, 229.
- McWilliam, A. 1991, *AJ*, 101, 1065.
- Meléndez, J., Barbuy, B., 2005, in preparation.
- Meynet, G., Maeder, A., 2000, *A&A*, 361, 101.
- Milone, A., Barbuy, B., Spite, M., Spite, F., 1992, *A&A*, 261, 551.
- Plez, B. and Brett, J.M. and Nordlund, A., 1992, *A&A*, 256, 551.
- Praderie, F., 1967, *Ann. Astrophys.*, 30, 31.
- Rieke, G.H., Lebofsky, M.J., 1985, *ApJ*, 288, 618.
- Royer, F., Gerbaldi, M., Faraggiana, R., Gómez, A., 2002, *A&A*, 381, 105.
- Sasselov, D.D., 1986, *PASP*, 98, 561.
- Schaller, G., Schaerer, D., Meynet, G., Maeder, M., 1992, *A&AS*, 96, 269.
- Spite, M., Barbuy, B., Spite, F., 1989, *A&A*, 222, 35.
- Takeda, Y., Takada-Hidai, M., 1998, *PASJ*, 50, 629.
- Usenko, I.A., Kovtyukh, V.V., Klochkova, V.G., 2001a, *A&A*, 377, 156.
- Usenko, I.A., Kovtyukh, V.V., Klochkova, V.G., Panchuk, V.E., Yermakov, S.V., 2001b, *A&A*, 367, 831.
- van Belle, G.T., Lane, B.F., Thompson, R.R. et al., 1999, *AJ*, 117, 521.
- Venn, K., 1995a, *ApJ*, 449, 839.
- Venn, K., 1995b, *ApJS*, 99, 659.
- Venn, K., 1999, *ApJ*, 518, 405.
- Venn, K., Brooks, A.M., Lambert, D.L., Lemke, M., Langer, N., Lennon, D.J., Keenan, F.P., 2002, *ApJ*, 565, 571.
- Xu, H.Y., Li, Y., 2004, *A&A*, 418, 213.

# Online Material

**Table 12.** FeI and FeII equivalent widths for the stars HD1219, HD36673, HD38713, HD44362, and HD45348

$\lambda$	Species	HD1219	HD36673	HD38713	HD44362	HD45348
5256.94	FE2	–	98.7	53.1	106.0	65.8
5264.81	FE2	71.0	192.3	86.5	192.1	–
5276.00	FE2	–	331.4	203.9	–	–
5284.11	FE2	84.8	211.3	105.9	218.9	161.0
5320.040	FE1	–	–	44.7	–	–
5321.109	FE1	78.6	10.2	67.2	–	–
5325.56	FE2	60.1	172.7	85.6	182.0	127.7
5337.73	FE2	–	–	–	142.7	–
5362.87	FE2	158.3	259.4	166.6	267.5	–
5364.880	FE1	162.1	91.9	151.9	197.4	86.0
5365.407	FE1	–	30.9	113.0	145.7	23.7
5367.476	FE1	170.7	114.0	159.3	206.4	110.5
5369.974	FE1	205.9	123.2	179.4	241.4	127.1
5373.714	FE1	100.9	23.6	91.5	109.1	31.4
5379.581	FE1	111.7	25.9	102.1	108.6	15.0
5383.380	FE1	205.4	137.8	197.9	246.6	142.0
5386.340	FE1	79.4	1.8	60.8	53.8	6.6
5389.486	FE1	–	50.9	120.4	156.7	56.8
5393.176	FE1	202.3	82.8	183.3	–	80.8
5395.222	FE1	–	–	–	–	–
5397.623	FE1	–	–	–	–	7.6
5398.287	FE1	114.9	34.4	105.4	130.0	43.7
5400.511	FE1	–	74.5	189.7	–	57.9
5412.791	FE1	62.4	–	44.8	–	–
5414.07	FE2	50.5	121.9	65.8	138.3	88.8
5425.26	FE2	65.7	165.5	76.7	167.5	121.3
5432.97	FE2	–	142.6	–	–	–
5436.297	FE1	77.7	–	66.5	–	–
5473.168	FE1	–	–	41.8	–	–
5483.108	FE1	–	7.9	72.1	–	15.7
5491.845	FE1	47.6	–	25.3	–	–
5494.474	FE1	73.5	–	55.3	–	–
5506.791	FE1	257.4	76.1	215.9	290.7	90.0
5522.454	FE1	83.6	–	69.3	54.5	13.6
5525.13	FE2	–	66.5	39.4	72.9	47.6
5525.552	FE1	99.7	–	83.1	81.6	20.6
5531.985	FE1	–	–	30.8	–	–
5534.848	FE2	–	225.0	100.4	226.9	223.9
5539.291	FE1	66.5	–	38.6	–	–
5543.944	FE1	99.1	–	85.4	90.7	38.9
5546.514	FE1	–	16.3	71.2	68.6	–
5560.207	FE1	–	19.9	76.7	76.2	–
5577.013	FE1	–	–	–	–	–
5587.573	FE1	81.5	–	64.0	–	–
5635.824	FE1	–	–	–	–	–
5636.705	FE1	66.5	–	45.5	–	–
5638.262	FE1	125.9	37.2	108.5	137.5	27.5
5641.436	FE1	–	–	–	106.0	19.2
5646.697	FE1	42.3	–	–	–	–
5650.019	FE1	72.1	–	57.5	–	11.0
5652.319	FE1	67.9	–	48.9	36.2	–
5661.348	FE1	–	–	49.3	36.4	–
5680.240	FE1	–	–	–	–	–
5701.557	FE1	157.9	24.1	128.6	–	19.0

**Table 12.** continued.

$\lambda$	Species	HD1219	HD36673	HD38713	HD44362	HD45348
5705.473	FE1	79.8	–	61.2	50.6	–
5731.761	FE1	96.1	18.9	89.7	87.3	–
5738.240	FE1	51.9	–	26.8	–	–
5778.463	FE1	82.1	–	54.5	–	–
5784.666	FE1	82.6	–	58.8	–	–
5811.916	FE1	–	–	26.9	–	–
5814.805	FE1	62.5	–	45.3	34.4	–
5835.098	FE1	51.8	–	–	–	–
6012.212	FE1	–	–	55.6	–	–
6079.014	FE1	79.1	14.5	73.1	–	–
6084.10	FE2	43.4	104.5	57.4	111.9	70.5
6093.666	FE1	66.7	–	53.7	41.8	5.4
6098.250	FE1	53.4	–	–	–	5.1
6113.33	FE2	27.9	66.6	39.7	–	43.2
6120.249	FE1	–	–	33.5	–	–
6129.70	FE2	–	32.7	–	–	20.6
6136.615	FE1	–	81.1	186.6	234.3	65.3
6137.002	FE1	142.1	–	118.5	–	10.9
6137.702	FE1	250.2	72.6	207.6	266.3	67.9
6141.03	FE2	17.2	14.8	15.2	–	150.2
6149.25	FE2	46.4	160.6	74.3	164.3	115.2
6151.616	FE1	–	–	98.2	87.1	–
6157.733	FE1	–	28.4	101.4	119.0	18.9
6159.382	FE1	48.9	–	29.8	–	–
6165.363	FE1	87.3	9.6	77.5	66.2	–
6170.500	FE1	–	31.3	–	115.2	26.0
6173.341	FE1	137.7	20.6	118.1	125.0	–
6179.39	FE2	–	41.6	–	–	25.9
6187.987	FE1	93.9	–	79.8	71.5	–
6191.558	FE1	–	88.9	183.1	227.8	56.5
6213.428	FE1	156.0	–	–	154.4	–
6226.730	FE1	72.1	–	56.8	–	–
6238.39	FE2	63.9	–	85.2	172.7	130.4
6239.95	FE2	–	–	–	–	58.5
6240.645	FE1	–	–	–	84.2	–
6247.55	FE2	53.8	–	89.7	219.2	–
6248.90	FE2	–	–	–	–	–
6271.283	FE1	75.6	–	52.0	–	–
6290.974	FE1	–	–	–	87.9	14.8
6293.933	FE1	–	–	–	–	–
6297.799	FE1	149.3	13.9	–	142.8	–
6301.508	FE1	167.8	–	163.0	–	63.7
6302.499	FE1	134.8	29.2	–	–	19.3
6305.314	FE2	–	–	–	38.4	–
6307.854	FE1	–	–	–	–	–
6315.314	FE1	–	–	–	–	–
6315.814	FE1	93.3	9.2	79.5	–	15.2
6322.694	FE1	143.3	24.5	–	135.4	9.7
6331.95	FE2	–	44.4	–	–	35.9
6336.823	FE1	–	45.2	136.2	161.9	37.8
6369.46	FE2	30.8	96.3	50.6	106.5	68.4
6380.750	FE1	103.1	–	82.3	75.1	19.0
6383.72	FE2	–	74.1	–	–	–
6385.45	FE2	–	56.5	–	–	32.3
6385.726	FE1	39.2	–	–	–	–

**Table 12.** continued.

$\lambda$	Species	HD1219	HD36673	HD38713	HD44362	HD45348
6392.538	FE1	80.8	–	–	–	–
6393.602	FE1	–	83.3	180.3	233.0	60.1
6400.000	FE1	–	92.1	173.4	–	68.6
6411.658	FE1	193.7	73.7	160.7	192.1	77.9
6416.92	FE2	57.1	169.9	68.4	156.9	118.8
6419.956	FE1	128.8	57.8	–	132.1	51.8
6421.360	FE1	200.7	62.6	220.5	239.0	50.1
6430.856	FE1	231.9	60.7	181.6	237.6	50.5
6432.68	FE2	56.9	153.7	82.7	170.5	113.5
6442.94	FE2	–	52.5	–	–	36.7
6446.40	FE2	–	48.8	8.0	–	33.8
6456.39	FE2	68.8	–	105.7	254.5	–

**Table 13.** FeI and FeII equivalent widths for the stars HD49068, HD49396, HD51043, HD66190, and HD71181

$\lambda$	Species	HD49068	HD49396	HD51043	HD66190	HD71181
5256.94	FE2	–	128.0	76.3	86.1	79.5
5264.81	FE2	78.0	225.9	123.7	124.1	113.9
5276.00	FE2	–	–	–	–	257.2
5284.11	FE2	103.8	228.7	–	149.3	154.1
5320.040	FE1	75.5	–	–	–	–
5321.109	FE1	92.3	98.6	95.8	107.6	–
5325.56	FE2	80.9	–	120.7	129.0	123.1
5337.73	FE2	–	–	–	99.3	–
5362.87	FE2	178.4	303.8	219.7	230.6	211.9
5364.880	FE1	168.3	300.1	192.4	229.6	183.0
5365.407	FE1	141.1	188.1	158.1	183.7	149.8
5367.476	FE1	185.8	307.9	222.4	248.0	190.6
5369.974	FE1	227.6	314.9	231.0	304.8	215.3
5373.714	FE1	115.3	134.0	123.7	143.0	112.4
5379.581	FE1	137.5	155.8	140.8	163.3	123.0
5383.380	FE1	241.5	331.9	260.4	299.5	210.5
5386.340	FE1	84.6	87.2	81.8	102.8	69.4
5389.486	FE1	145.9	198.3	152.3	175.8	140.0
5393.176	FE1	230.1	339.2	–	294.3	212.1
5395.222	FE1	–	–	52.0	–	45.9
5397.623	FE1	–	–	90.3	–	72.8
5398.287	FE1	127.8	169.7	140.1	169.0	121.1
5400.511	FE1	249.5	248.8	234.2	273.7	218.0
5412.791	FE1	61.8	–	–	86.1	52.6
5414.07	FE2	51.5	146.9	89.2	88.0	80.7
5425.26	FE2	68.7	186.9	116.9	106.4	–
5432.97	FE2	–	–	–	151.8	–
5436.297	FE1	78.4	–	–	–	74.1
5473.168	FE1	67.5	–	–	–	–
5483.108	FE1	–	–	–	–	–
5491.845	FE1	–	–	–	57.7	47.9
5494.474	FE1	79.1	79.8	76.2	98.9	83.3
5506.791	FE1	348.8	442.0	366.9	406.6	295.7
5522.454	FE1	91.8	115.4	103.0	127.4	91.6
5525.13	FE2	–	97.9	67.6	–	–
5525.552	FE1	115.6	144.7	120.4	139.7	110.0
5531.985	FE1	–	–	–	73.5	47.1
5534.848	FE2	111.4	341.0	155.2	182.4	156.9
5539.291	FE1	75.7	–	74.3	92.6	60.4
5543.944	FE1	112.3	143.4	119.9	143.5	115.7
5546.514	FE1	–	117.4	108.4	139.3	106.3
5560.207	FE1	–	111.8	102.4	118.0	91.7
5577.013	FE1	–	–	–	–	21.7
5587.573	FE1	89.5	–	82.8	–	74.4
5635.824	FE1	82.3	83.4	84.4	107.0	78.3
5636.705	FE1	77.7	–	66.6	96.6	64.8
5638.262	FE1	137.1	173.9	142.2	175.8	142.8
5641.436	FE1	–	139.1	131.6	161.5	128.7
5646.697	FE1	38.3	–	–	41.6	–
5650.019	FE1	76.7	–	80.9	90.9	70.5
5652.319	FE1	70.1	–	65.7	86.9	62.1
5661.348	FE1	–	64.0	73.3	96.9	62.0
5680.240	FE1	–	–	–	66.6	39.5
5701.557	FE1	185.9	215.2	186.1	232.3	181.1

**Table 13.** continued.

$\lambda$	Species	HD49068	HD49396	HD51043	HD66190	HD71181
5705.473	FE1	83.5	86.6	80.5	104.7	85.2
5731.761	FE1	120.2	136.3	121.9	144.2	109.5
5738.240	FE1	55.0	–	43.6	–	36.1
5778.463	FE1	100.6	72.0	–	116.3	79.1
5784.666	FE1	93.4	–	82.3	108.2	75.6
5811.916	FE1	44.4	–	–	51.4	35.0
5814.805	FE1	71.0	59.7	–	78.8	56.6
5835.098	FE1	–	–	–	–	40.2
6012.212	FE1	98.3	–	–	124.4	84.8
6079.014	FE1	94.0	99.0	95.4	120.7	87.5
6084.10	FE2	54.4	129.7	84.5	89.5	82.8
6093.666	FE1	76.5	64.2	71.6	88.1	67.4
6098.250	FE1	62.7	–	–	75.5	48.1
6113.33	FE2	47.0	–	–	79.0	59.4
6120.249	FE1	–	–	–	99.4	51.1
6129.70	FE2	–	–	–	–	–
6136.615	FE1	258.5	–	257.0	–	246.3
6137.002	FE1	171.6	–	156.5	–	155.4
6137.702	FE1	307.5	340.1	304.7	367.3	268.7
6141.03	FE2	21.5	–	–	–	–
6149.25	FE2	64.8	178.4	109.2	106.5	97.7
6151.616	FE1	148.7	152.1	–	–	128.5
6157.733	FE1	150.7	172.8	151.1	189.8	142.3
6159.382	FE1	52.2	–	46.5	61.5	36.2
6165.363	FE1	99.6	109.7	101.2	127.5	94.4
6170.500	FE1	–	171.3	160.7	–	157.6
6173.341	FE1	185.7	218.5	161.9	250.6	171.5
6179.39	FE2	–	–	–	–	–
6187.987	FE1	108.3	117.8	–	130.0	99.0
6191.558	FE1	–	–	–	–	259.9
6213.428	FE1	196.6	222.9	189.8	239.9	191.2
6226.730	FE1	–	71.2	–	94.8	73.5
6238.39	FE2	89.0	195.7	–	128.2	117.7
6239.95	FE2	–	–	–	–	–
6240.645	FE1	145.1	148.3	–	185.6	137.3
6247.55	FE2	74.3	239.6	–	–	129.1
6248.90	FE2	–	–	–	–	–
6271.283	FE1	92.2	–	77.1	105.7	78.8
6290.974	FE1	–	131.2	–	147.2	–
6293.933	FE1	–	–	–	–	–
6297.799	FE1	221.1	201.8	185.5	269.8	183.6
6301.508	FE1	223.3	–	220.9	274.8	185.6
6302.499	FE1	150.1	191.2	155.7	223.1	157.5
6305.314	FE2	–	–	–	–	–
6307.854	FE1	–	–	–	–	–
6315.314	FE1	152.2	–	–	174.0	–
6315.814	FE1	111.0	129.7	99.3	127.3	93.9
6322.694	FE1	191.0	200.6	170.9	265.6	165.7
6331.95	FE2	–	–	–	–	–
6336.823	FE1	195.5	227.4	194.8	232.4	183.1
6369.46	FE2	44.4	126.3	72.3	75.8	73.5
6380.750	FE1	120.8	128.5	119.2	147.3	115.1
6383.72	FE2	–	–	–	–	–
6385.45	FE2	–	–	–	–	–
6385.726	FE1	37.6	–	–	–	–

**Table 13.** continued.

$\lambda$	Species	HD49068	HD49396	HD51043	HD66190	HD71181
6392.538	FE1	97.8	65.1	–	119.6	76.0
6393.602	FE1	267.2	–	262.0	337.6	256.3
6400.000	FE1	220.9	–	–	–	–
6411.658	FE1	215.2	284.6	216.2	281.4	201.2
6416.92	FE2	67.8	–	91.9	101.2	94.3
6419.956	FE1	146.1	173.5	146.5	182.5	147.4
6421.360	FE1	313.4	325.5	–	333.5	248.1
6430.856	FE1	291.2	343.0	279.1	351.0	248.9
6432.68	FE2	69.3	182.3	114.9	117.3	113.8
6442.94	FE2	11.7	30.1	17.0	–	–
6446.40	FE2	7.4	–	–	–	–
6456.39	FE2	98.4	272.2	–	153.8	151.0



**Table 14.** FeI and FeII equivalent widths for the stars HD76860, HD80404, HD90289, HD102839, and HD114792

$\lambda$	Species	HD71860	HD80404	HD90289	HD102839	HD114792
5256.94	FE2	77.7	–	–	109.6	126.2
5264.81	FE2	90.4	132.6	49.3	131.1	–
5276.00	FE2	–	–	206.6	–	–
5284.11	FE2	113.5	148.7	64.3	–	241.2
5320.040	FE1	–	–	77.5	–	–
5321.109	FE1	124.1	–	87.0	–	–
5325.56	FE2	101.7	117.4	54.2	173.0	198.2
5337.73	FE2	77.0	–	–	–	165.7
5362.87	FE2	213.9	181.2	–	268.1	296.9
5364.880	FE1	208.5	71.4	–	242.1	221.2
5365.407	FE1	186.9	23.0	–	212.3	162.4
5367.476	FE1	209.0	103.5	–	251.8	224.0
5369.974	FE1	269.9	105.9	171.4	267.6	252.4
5373.714	FE1	148.3	19.8	100.9	153.5	108.3
5379.581	FE1	166.0	–	109.2	171.0	–
5383.380	FE1	282.9	120.7	201.9	281.0	252.0
5386.340	FE1	102.2	–	68.5	102.1	–
5389.486	FE1	181.2	36.1	133.9	201.0	159.9
5393.176	FE1	279.5	–	218.6	295.0	266.1
5395.222	FE1	78.7	–	56.5	–	31.9
5397.623	FE1	–	–	–	–	–
5398.287	FE1	163.1	26.2	104.1	171.2	135.6
5400.511	FE1	–	52.6	–	–	215.6
5412.791	FE1	91.7	–	–	76.8	–
5414.07	FE2	–	79.6	–	102.7	144.5
5425.26	FE2	76.9	109.6	40.0	131.0	189.2
5432.97	FE2	168.5	89.2	–	170.5	174.6
5436.297	FE1	–	–	77.1	–	–
5473.168	FE1	80.2	–	–	–	–
5483.108	FE1	–	–	81.3	–	–
5491.845	FE1	–	–	40.2	67.5	–
5494.474	FE1	96.8	–	78.1	–	–
5506.791	FE1	–	53.7	396.1	477.2	306.4
5522.454	FE1	125.1	–	84.0	134.6	80.6
5525.13	FE2	–	44.4	–	–	99.5
5525.552	FE1	144.1	11.8	103.2	170.1	105.2
5531.985	FE1	–	–	–	–	32.4
5534.848	FE2	–	189.4	–	236.4	259.8
5539.291	FE1	111.0	–	71.0	96.6	40.9
5543.944	FE1	146.3	21.6	100.3	163.7	115.9
5546.514	FE1	146.3	–	90.4	–	97.4
5560.207	FE1	–	–	76.4	127.3	88.5
5577.013	FE1	–	–	23.3	–	–
5587.573	FE1	96.2	–	71.8	–	–
5635.824	FE1	108.7	–	76.9	–	–
5636.705	FE1	107.5	–	69.4	99.4	49.0
5638.262	FE1	180.2	24.9	123.8	193.5	152.2
5641.436	FE1	169.8	–	117.7	168.3	120.3
5646.697	FE1	54.9	–	36.8	33.1	–
5650.019	FE1	99.1	–	66.1	93.4	–
5652.319	FE1	96.6	–	61.2	85.6	45.0
5661.348	FE1	–	–	–	85.6	–
5680.240	FE1	–	–	47.7	–	–
5701.557	FE1	–	–	179.6	267.3	174.3

**Table 14.** continued.

$\lambda$	Species	HD76860	HD80404	HD90289	HD102839	HD114792
5705.473	FE1	115.1	–	74.7	117.2	72.3
5731.761	FE1	153.0	–	99.8	151.3	105.4
5738.240	FE1	66.1	–	58.6	59.4	–
5778.463	FE1	145.5	–	100.0	126.2	49.6
5784.666	FE1	128.2	–	89.6	111.1	–
5811.916	FE1	55.2	–	38.5	51.9	–
5814.805	FE1	90.7	–	67.1	81.5	41.6
5835.098	FE1	–	–	45.4	64.8	–
6012.212	FE1	146.8	–	102.0	132.2	–
6079.014	FE1	106.5	13.6	75.4	125.0	78.5
6084.10	FE2	69.2	67.6	–	113.7	132.5
6093.666	FE1	89.5	–	62.2	94.2	57.6
6098.250	FE1	88.0	–	57.0	–	43.7
6113.33	FE2	–	42.3	–	95.1	98.0
6120.249	FE1	–	–	103.2	–	–
6129.70	FE2	–	20.9	–	–	–
6136.615	FE1	–	53.1	251.2	–	–
6137.002	FE1	–	–	159.2	–	–
6137.702	FE1	464.8	58.6	281.1	384.7	271.0
6141.03	FE2	–	7.1	8.6	–	–
6149.25	FE2	82.9	109.6	–	135.9	180.4
6151.616	FE1	–	–	142.1	205.9	111.3
6157.733	FE1	230.7	–	130.4	204.9	140.1
6159.382	FE1	70.1	–	53.3	55.2	19.5
6165.363	FE1	132.6	4.8	90.6	135.8	82.7
6170.500	FE1	–	–	–	234.7	142.9
6173.341	FE1	289.1	–	164.6	262.6	166.4
6179.39	FE2	–	27.4	–	–	–
6187.987	FE1	141.1	–	101.5	142.1	86.6
6191.558	FE1	–	54.2	–	–	–
6213.428	FE1	–	27.0	179.8	274.7	191.2
6226.730	FE1	98.9	–	80.8	106.3	–
6238.39	FE2	–	–	–	–	191.6
6239.95	FE2	–	50.0	–	–	101.0
6240.645	FE1	209.6	–	139.5	216.0	110.9
6247.55	FE2	83.4	–	49.0	170.0	237.3
6248.90	FE2	–	35.5	–	–	27.4
6271.283	FE1	120.8	–	82.2	114.9	–
6290.974	FE1	145.4	18.0	–	163.8	–
6293.933	FE1	–	–	34.7	–	–
6297.799	FE1	292.3	–	184.3	274.9	175.9
6301.508	FE1	246.6	41.5	156.0	263.3	213.6
6302.499	FE1	198.2	25.1	133.5	221.0	–
6305.314	FE2	–	–	–	–	–
6307.854	FE1	–	–	33.3	–	–
6315.314	FE1	186.3	–	–	179.4	–
6315.814	FE1	131.4	–	84.9	129.6	–
6322.694	FE1	250.8	–	158.8	249.6	155.8
6331.95	FE2	–	36.9	–	–	–
6336.823	FE1	–	30.8	152.8	256.5	190.9
6369.46	FE2	63.8	65.4	28.8	102.4	124.7
6380.750	FE1	164.7	–	–	159.3	92.4
6383.72	FE2	–	58.9	–	–	46.3
6385.45	FE2	–	–	–	–	–
6385.726	FE1	55.8	–	–	43.0	–

**Table 14.** continued.

$\lambda$	Species	HD76860	HD80404	HD90289	HD102839	HD114792
6392.538	FE1	–	–	92.6	127.3	–
6393.602	FE1	–	46.7	249.3	–	268.4
6400.000	FE1	–	60.2	183.6	–	–
6411.658	FE1	268.6	53.9	174.6	273.2	217.2
6416.92	FE2	81.0	105.4	–	125.1	165.2
6419.956	FE1	182.2	46.2	110.9	207.2	153.3
6421.360	FE1	359.1	40.7	286.4	359.9	–
6430.856	FE1	418.1	43.2	306.0	385.2	254.1
6432.68	FE2	80.1	97.4	54.8	148.2	189.3
6442.94	FE2	–	34.1	–	–	26.9
6446.40	FE2	–	31.0	–	–	–
6456.39	FE2	113.7	177.0	50.1	199.4	279.2

**Table 15.** FeI and FeII equivalent widths for the stars HD159633, HD192876, HD204867, and HD225212

$\lambda$	Species	HD159633	HD192876	HD204860	HD225212
5256.94	FE2	129.4	97.4	120.0	86.4
5264.81	FE2	216.2	168.0	220.1	81.4
5276.00	FE2	–	–	–	–
5284.11	FE2	214.1	196.4	237.5	–
5320.040	FE1	–	–	–	–
5321.109	FE1	86.8	86.2	–	147.2
5325.56	FE2	–	159.7	201.1	117.8
5337.73	FE2	–	–	165.6	85.8
5362.87	FE2	303.1	259.7	291.3	243.3
5364.880	FE1	251.9	205.1	214.2	226.2
5365.407	FE1	197.7	165.3	153.2	204.6
5367.476	FE1	258.7	211.2	225.2	222.7
5369.974	FE1	270.4	230.5	253.2	243.8
5373.714	FE1	155.1	124.7	108.4	165.2
5379.581	FE1	168.0	134.9	112.1	176.3
5383.380	FE1	287.1	–	247.5	271.6
5386.340	FE1	99.0	84.1	64.0	113.1
5389.486	FE1	199.4	171.0	165.7	187.8
5393.176	FE1	313.8	254.8	266.6	278.9
5395.222	FE1	–	–	–	97.4
5397.623	FE1	519.5	60.3	–	–
5398.287	FE1	181.3	151.8	141.5	174.9
5400.511	FE1	258.9	235.0	204.8	–
5412.791	FE1	–	–	–	–
5414.07	FE2	145.1	113.5	149.4	70.9
5425.26	FE2	178.5	140.8	183.9	–
5432.97	FE2	–	158.6	176.1	–
5436.297	FE1	–	82.6	–	–
5473.168	FE1	–	–	–	98.2
5483.108	FE1	–	–	–	–
5491.845	FE1	–	32.2	–	–
5494.474	FE1	–	74.2	46.9	–
5506.791	FE1	455.3	350.0	311.2	–
5522.454	FE1	117.2	100.8	77.7	138.5
5525.13	FE2	94.5	73.6	85.8	80.3
5525.552	FE1	141.9	–	103.9	159.6
5531.985	FE1	–	–	–	–
5534.848	FE2	267.5	213.9	255.0	–
5539.291	FE1	67.2	58.1	33.0	123.6
5543.944	FE1	144.4	124.4	105.8	154.9
5546.514	FE1	131.1	108.9	84.2	168.4
5560.207	FE1	120.9	100.3	80.9	–
5577.013	FE1	–	–	–	34.7
5587.573	FE1	–	–	–	–
5635.824	FE1	–	–	–	117.8
5636.705	FE1	69.9	62.4	–	116.7
5638.262	FE1	180.4	155.6	140.3	191.6
5641.436	FE1	151.9	132.4	108.7	182.8
5646.697	FE1	–	–	–	58.2
5650.019	FE1	80.5	72.2	–	–
5652.319	FE1	65.1	58.2	35.8	97.5
5661.348	FE1	72.4	62.7	33.9	128.2
5680.240	FE1	–	–	–	86.8
5701.557	FE1	227.9	192.4	160.9	–

**Table 15.** continued.

$\lambda$	Species	HD159633	HD192876	HD204860	HD225212
5705.473	FE1	95.4	82.5	58.5	121.0
5731.761	FE1	130.5	116.3	92.1	154.5
5738.240	FE1	–	–	–	88.4
5778.463	FE1	87.8	74.8	38.4	160.5
5784.666	FE1	–	73.9	45.4	140.1
5811.916	FE1	30.9	35.4	–	68.4
5814.805	FE1	58.2	56.5	35.5	96.8
5835.098	FE1	–	–	–	95.7
6012.212	FE1	–	–	–	168.8
6079.014	FE1	106.4	93.1	64.8	121.3
6084.10	FE2	136.6	107.6	133.7	78.6
6093.666	FE1	74.6	65.2	–	–
6098.250	FE1	–	–	–	98.6
6113.33	FE2	102.6	81.9	89.4	–
6120.249	FE1	–	40.7	–	183.2
6129.70	FE2	–	–	64.0	–
6136.615	FE1	–	–	–	–
6137.002	FE1	–	–	–	–
6137.702	FE1	349.2	290.0	252.9	457.4
6141.03	FE2	–	–	–	–
6149.25	FE2	172.1	137.2	171.2	90.9
6151.616	FE1	161.8	–	94.0	243.0
6157.733	FE1	176.6	153.8	120.0	230.2
6159.382	FE1	39.6	38.0	22.2	91.0
6165.363	FE1	111.6	101.0	70.3	150.3
6170.500	FE1	188.0	158.2	130.0	–
6173.341	FE1	216.6	176.3	142.7	297.3
6179.39	FE2	–	–	–	–
6187.987	FE1	115.1	–	76.1	153.0
6191.558	FE1	–	265.4	–	–
6213.428	FE1	239.5	196.6	165.2	–
6226.730	FE1	83.5	72.7	55.3	132.4
6238.39	FE2	198.8	154.7	191.5	–
6239.95	FE2	–	–	103.0	–
6240.645	FE1	171.7	138.8	99.8	239.5
6247.55	FE2	234.8	185.1	240.7	103.7
6248.90	FE2	–	–	36.8	–
6271.283	FE1	–	–	–	156.8
6290.974	FE1	143.4	–	–	174.0
6293.933	FE1	–	–	–	–
6297.799	FE1	267.5	189.3	150.1	320.9
6301.508	FE1	248.5	213.8	209.8	264.3
6302.499	FE1	204.6	182.1	149.3	228.4
6305.314	FE2	–	–	–	–
6307.854	FE1	–	–	–	68.6
6315.314	FE1	–	150.8	–	206.4
6315.814	FE1	112.1	109.3	77.5	150.6
6322.694	FE1	224.6	180.6	147.2	277.3
6331.95	FE2	–	–	53.6	–
6336.823	FE1	–	197.6	184.6	270.0
6369.46	FE2	119.5	97.9	117.5	58.5
6380.750	FE1	232.0	111.4	82.1	–
6383.72	FE2	–	–	49.7	–
6385.45	FE2	–	–	–	–
6385.726	FE1	–	–	–	58.7

**Table 15.** continued.

$\lambda$	Species	HD159633	HD192876	HD204860	HD225212
6392.538	FE1	74.3	66.6	33.3	–
6393.602	FE1	–	–	246.8	–
6400.000	FE1	–	–	–	–
6411.658	FE1	262.4	225.2	214.3	271.6
6416.92	FE2	165.5	134.1	175.3	93.8
6419.956	FE1	203.6	164.4	144.8	208.4
6421.360	FE1	344.2	299.2	236.0	387.9
6430.856	FE1	362.2	268.5	238.3	499.0
6432.68	FE2	186.6	154.4	189.4	97.5
6442.94	FE2	–	–	30.2	–
6446.40	FE2	–	–	–	–
6456.39	FE2	268.9	214.9	277.8	108.4